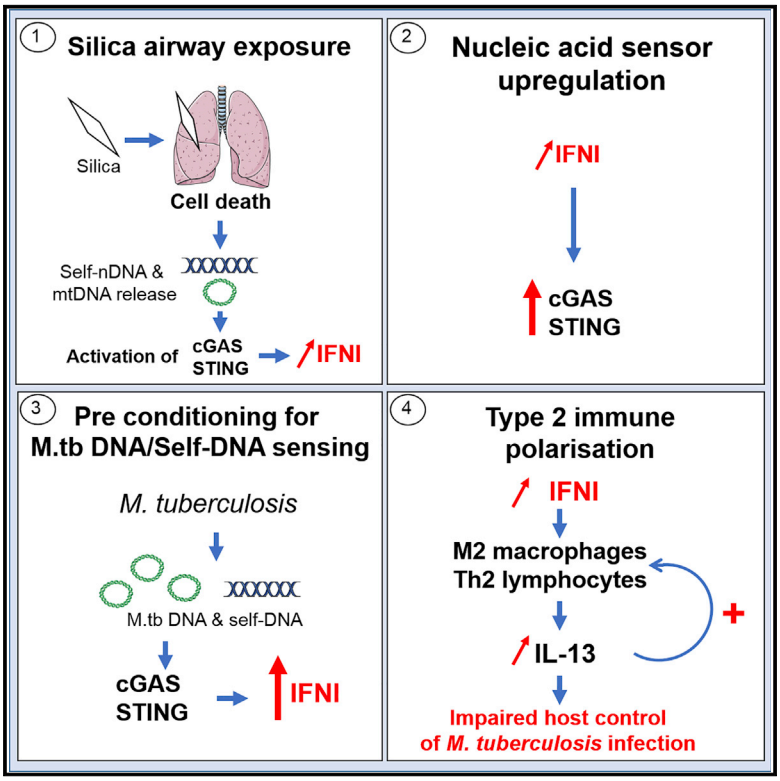
Article

Cell Reports

Sterile Lung Inflammation Induced by Silica Exacerbates *Mycobacterium tuberculosis* Infection via STING-Dependent Type 2 Immunity

Graphical Abstract



Highlights

- Silica impairs host control of *M. tuberculosis* infection via a type 2 immune response
- Extracellular DNA potentiates silica-induced exacerbation of *M. tuberculosis* infection
- Silica primes STING activation, potentiating the response to *M. tuberculosis* DNA
- Both host and *M. tuberculosis* DNA trigger cGAS/STING/IFNI-mediated type 2 immunity

Authors

Sulayman Benmerzoug, Badreddine Bounab, Stéphanie Rose, ..., Bernhard Ryffel, Dieudonnee Togbe, Valerie F.J. Quesniaux

Correspondence

quesniaux@cnrs-orleans.fr

In Brief

Benmerzoug et al. mechanistically dissect how sterile lung inflammation induced by silica exacerbates *M. tuberculosis* infection (silicotuberculosis). Silica exposure induces self-dsDNA release and STING pathway activation, which potentiate the host response to *M. tuberculosis* DNA via initiation of type 2 immunity. Thus, STING and nucleic acids represent interesting therapeutic targets for silicotuberculosis.

Benmerzoug et al., 2019, Cell Reports *27*, 2649–2664
May 28, 2019 © 2019 The Author(s).
https://doi.org/10.1016/j.celrep.2019.04.110

CellPress

Cell Reports
Article

OPEN ACCESS
CellPress

Sterile Lung Inflammation Induced by Silica Exacerbates *Mycobacterium tuberculosis* Infection via STING-Dependent Type 2 Immunity

Sulayman Benmerzoug,[1,2] Badreddine Bounab,[1,2] Stéphanie Rose,[1,2] David Gosset,[3] Franck Biet,[4] Thierry Cochard,[4] Aurore Xavier,[1,2] Nathalie Rouxel,[5] Louis Fauconnier,[5] William G.C. Horsnell,[1,2,6,7,8] Bernhard Ryffel,[1,2,6] Dieudonnee Togbe,[5] and Valerie F.J. Quesniaux[1,2,9,*]

[1]CNRS, UMR7355, Orléans 45071, France
[2]Experimental and Molecular Immunology and Neurogenetics, University of Orléans, Orléans 45071, France
[3]Center for Molecular Biophysics, CNRS UPR4301, Orléans 45071, France
[4]Institut National de la Recherche Agronomique, Université de Tours, UMR1282, Infectiologie et Santé Publique, Nouzilly 37380, France
[5]Artimmune SAS, 13 Avenue Buffon, Orléans-Cedex 2 45071, France
[6]Institute of Infectious Disease and Molecular Medicine, University of Cape Town, Cape Town 7925, South Africa
[7]Institute of Microbiology and Infection, University of Birmingham, Birmingham B15 2TT, UK
[8]Le Studium Institute for Advanced Studies, Rue Dupanloup, Orléans 45000, France
[9]Lead Contact
*Correspondence: quesniaux@cnrs-orleans.fr
https://doi.org/10.1016/j.celrep.2019.04.110

SUMMARY

Lung inflammation induced by silica impairs host control of tuberculosis, yet the underlying mechanism remains unclear. Here, we show that silica-driven exacerbation of *M. tuberculosis* infection associates with raised type 2 immunity. Silica increases pulmonary Th2 cell and M2 macrophage responses, while reducing type 1 immunity after *M. tuberculosis* infection. Silica induces lung damage that prompts extracellular self-DNA release and activates STING. This STING priming potentiates *M. tuberculosis* DNA sensing by and activation of cGAS/STING, which triggers enhanced type I interferon (IFNI) response and type 2 immunity. cGAS-, STING-, and IFNAR-deficient mice are resistant to silica-induced exacerbation of *M. tuberculosis* infection. Thus, silica-induced self-DNA primes the host response to *M. tuberculosis*-derived nucleic acids, which increases type 2 immunity while reducing type 1 immunity, crucial for controlling *M. tuberculosis* infection. These data show how cGAS/STING pathway activation, at the crossroads of sterile inflammation and infection, may affect the host response to pathogens such as *M. tuberculosis*.

INTRODUCTION

Occupational and environmental exposures to silica affect lung function with a significant, yet underappreciated, influence on global respiratory health (Quail, 2017). Silica exposure also exacerbates comorbidities, including an up to 40-fold increased risk for pulmonary tuberculosis (Barboza et al., 2008; Calvert et al., 2003; Marcy, 1950; Melo et al., 2016). Fine particulate air pollutants have been associated with tuberculosis incidence and outcome (Popovic et al., 2019). However, the underlying mechanisms by which patients exposed to silica become predisposed to the development of severe tuberculosis are poorly understood (Konečný et al., 2019). Inhaled crystalline silica affects immune and non-immune cell types, resulting in responses ranging from inflammation to oxidative stress and cell death (Joshi and Knecht, 2013; Porter et al., 2004, 2006). In particular, silica induces nucleotide-binding oligomerization domain (NOD)-like receptor family, pyrin domain containing 3 (NLRP3) inflammasome activation and interleukin-1 (IL-1)-dependent inflammation (Hornung et al., 2008), but also type I interferons (IFNIs) that contribute to silica-induced chronic lung inflammation (Giordano et al., 2010).

Silica-induced inflammation may either enhance or antagonize canonical immune protective responses against *Mycobacterium tuberculosis* infection mediated by tumor necrosis factor (TNF), interferon (IFN)γ, IL-1, IL-12, and nitric oxide (Cliff et al., 2015; Cooper et al., 1997; Flynn et al., 1993; O'Garra et al., 2013). This protective anti-mycobacterial type 1 immune response is counteracted by the bacilli, which elicit deleterious IFNI- and IL-10-mediated responses, promoting permissive macrophages (Cambier et al., 2014; McNab et al., 2015; Moreira-Teixeira et al., 2018; O'Garra et al., 2013; Orme et al., 2015; Schreiber et al., 2009; Srivastava et al., 2014). *M. tuberculosis* residing in the macrophage release DNA, which is detected by the cytosolic surveillance system through cyclic guanosine monophosphate (cGMP)-AMP synthase (cGAS), triggering activation of the stimulator of IFN genes (STING) adaptor molecule and inducing IFNI responses (Collins et al., 2015; Manzanillo et al., 2012; Wassermann et al., 2015; Watson et al., 2015). While the STING pathway contributes to the host response to infection, including bacterial infections (Marinho et al., 2017), it does not seem essential to control *in vivo M. tuberculosis* infection (Collins et al., 2015; Marinho et al., 2018).

This is an open access article under the CC BY-NC-ND license (http://creativecommons.org/licenses/by-nc-nd/4.0/).

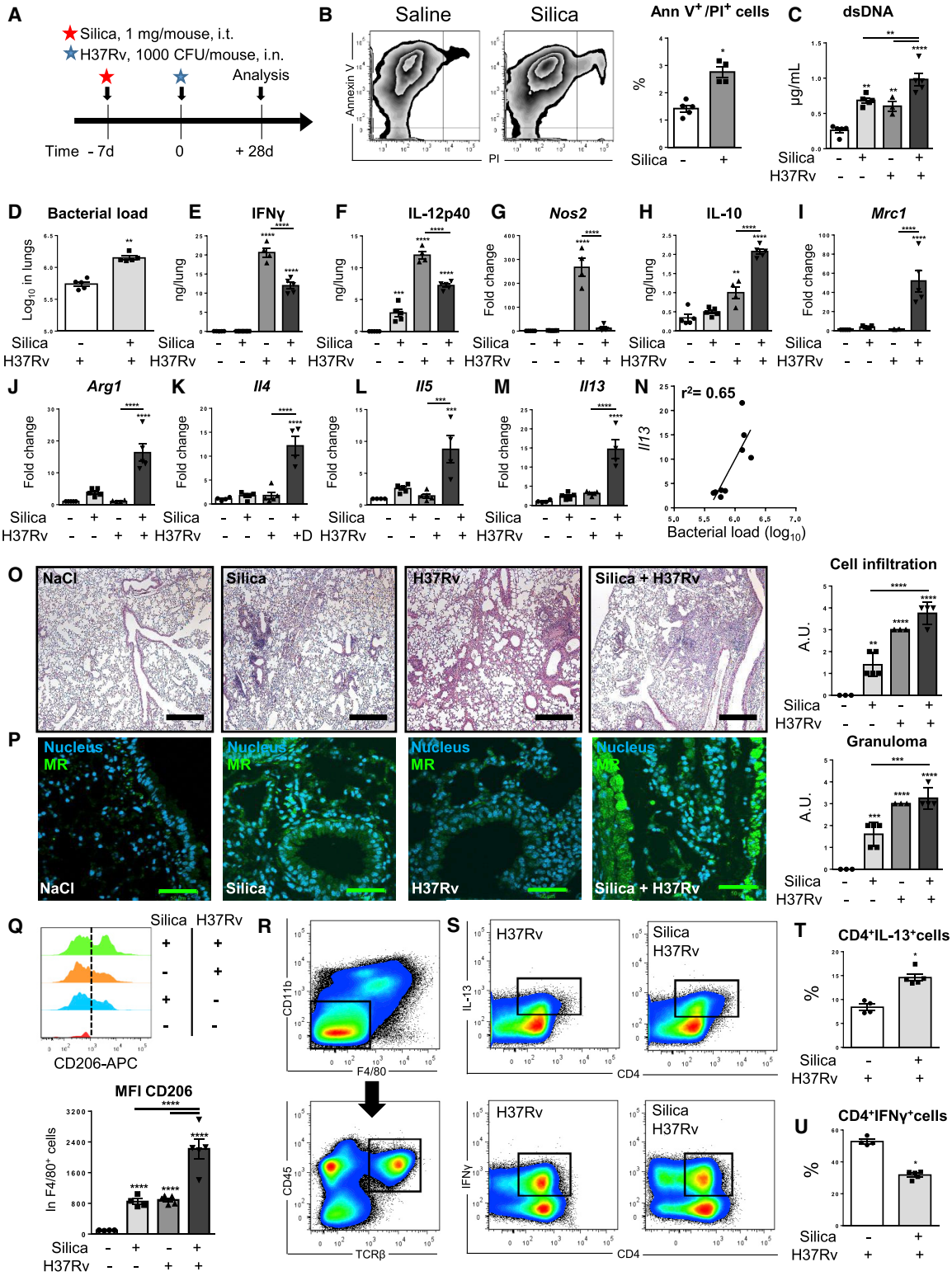


Figure 1. Silica Exacerbates Type 2 Immune Response after *M. tuberculosis* Infection

(A) Silica microparticles (1 mg/mouse, intratracheally [i.t.]) or saline vehicle was administered to WT mice 7 days before infection with *M. tuberculosis* H37Rv (1,000 CFU/mouse, intranasally [i.n.]). The parameters were analyzed in the lung on day 28 post-infection, unless otherwise stated.

(B) Flow cytometry analysis of bronchoalveolar cell death 7 days after silica exposure with a quantification of annexin V^+/PI^+ cells.

(legend continued on next page)

In the present study, we explore how silica pre-exposure compromises the host control of *M. tuberculosis* infection. We hypothesized that silica-induced cell damage, raising self-DNA-mediated release of IFNI through the STING pathway, may impair the host control of infection. Furthermore, we proposed that promoting pulmonary immunity to detect and respond to host nucleic acids may also increase the ability of the host to respond to pathogen-derived nucleic acids. This was the case, as silica pre-exposure upregulated the cGAS/STING DNA-sensing pathway. This potentiated the STING-dependent response to *M. tuberculosis*, leading to IFNI overexpression and raised type 2 immune responses, while decreasing type 1 immune response. DNA was central to this response, as it was recapitulated by *M. tuberculosis* DNA (*M.tb* DNA) administration in silica-pre-exposed mice. Thus, silica exposure through self-double-stranded DNA (dsDNA) release primes the host cytosolic surveillance system and conditions the host to fully respond to *M.tb* DNA, driving a cGAS/STING-dependent type 2 immunity that antagonizes the type 1 immunity, crucial for host control of *M. tuberculosis*. These data provide an underlying mechanism for silica exacerbation of *M. tuberculosis* infection and show the implication of nucleic acids in mycobacterial infection. The duality of the STING adaptor molecule, sensing nucleic acids from both the host and the pathogen, is central to explain silica-induced exacerbation of *M. tuberculosis* infection and shows how the activation of cGAS/STING by self-DNA may affect the host response to infection.

RESULTS

Silica Pre-exposure Exacerbates *M. tuberculosis* Infection and Type 2 Immune Response

Type 1 immunity is essential for the control of *M. tuberculosis* infection (O'Garra et al., 2013), and we asked whether silica pre-exposure could affect the immunological balance between type 1 and type 2 immune responses. Mice were pre-exposed intratracheally to silica microparticles 7 days before intranasal infection with *M. tuberculosis* H37Rv (Figure 1A). Silica exposure induced bronchoalveolar cell death (Figure 1B), with dsDNA release in the bronchoalveolar lavage fluid (BALF), which was more prominent after silica and *M. tuberculosis* infection (Figure 1C). Silica pre-exposure increased the mycobacterial burden in the lung 4 weeks post-infection (Figure 1D). IFNγ and IL-12p40, two major cytokines involved in the host control of *M. tuberculosis* infection, and inducible nitric oxide system (iNOS)-coding gene *Nos2*, leading to mycobactericidal nitric oxide (NO) production, were significantly decreased after silica exposure in *M. tuberculosis*-infected mice (Figures 1E–1G). Conversely, IL-10, mannose receptor (MR), and the arginase 1-coding genes *Mrc1* and *Arg1* were overexpressed after silica exposure in *M. tuberculosis*-infected mice (Figures 1H–1J), which is indicative of an alternative M2 response. Moreover, T helper 2 (Th2)-induced cytokine genes such as *Il4*, *Il5*, and *Il13* were upregulated in the lung upon silica exposure plus *M. tuberculosis* infection (Figures 1K–1M). We report here a positive correlation between *Il13* expression in the lungs and lung bacterial burden after *M. tuberculosis* infection, indicating that IL-13 may be detrimental to the host (Figure 1N). Silica exposure induced more severe tissue damage and cell infiltration in the lungs of *M. tuberculosis*-infected mice (Figure 1O), with raised MR expression, a hallmark of M2 macrophages, as compared with silica-exposed or *M. tuberculosis*-infected mice (Figures 1P and 1Q). We then asked whether the Th1/Th2 balance was affected by silica. After silica exposure, the proportion of IL-13$^+$CD4$^+$ Th2 cells was increased and, conversely, IFNγ$^+$CD4$^+$ Th1 cells were decreased in the lungs of *M. tuberculosis*-infected mice (Figures 1R–1U). Thus, silica exposure modified the balance of immune responses induced by *M. tuberculosis* infection, with increased type 2 immunity and reduced type 1 immunity, leading to impaired control of the infection.

IFNI and STING Pathways Are Overexpressed in Silica-Pre-exposed *M. tuberculosis*-Infected Mice

IFNI is associated with a defective control of *M. tuberculosis* infection (Mayer-Barber et al., 2014; O'Garra et al., 2013), and we next asked whether the IFNI pathway contributes to the silica-induced exacerbation of *M. tuberculosis* infection. *Ifnα* and *Ifnβ* gene expression was increased after silica exposure and *M. tuberculosis* infection (Figures 2A and 2B), and this correlated with raised bacterial burden in the lung on day 28 post-infection (Figures 2C and 2D). There was a strong positive correlation between *Ifnβ* and *Il13* expression in the lungs of these mice (Figure 2E). Silica pre-exposure also exacerbated the production of IFN-stimulated gene CXCL10 after *M. tuberculosis* infection (Figure 2F).

(C) Quantification of extracellular dsDNA in the acellular fractions of bronchoalveolar lavage fluid (BALF).
(D) Bacterial burden.
(E, F, and H) ELISA measurement of IFNγ (E), IL-12p40 (F), and IL-10 (H).
(G and I–M) mRNA levels of *Nos2* (G), *Mrc1* (I), *Arg1* (J), *Il4* (K), *Il5* (L), and *Il13* (M) assessed by qRT-PCR.
(N) Correlation between *Il13* expression and lung bacterial load.
(O) Lung tissue histology H&E staining, with pathology scoring of the presence of inflammatory cell infiltration and granuloma. Bars, 200μm.
(P) Confocal images of DNA dye Draq5 (blue) and mannose receptor (MR; green) staining. Bars, 50 μm.
(Q) Flow cytometry analysis of MR CD206 expression in CD45$^+$ F4/80$^+$ cells: histograms from individual mice and CD206 mean fluorescence intensity (MFI).
(R and S) Gating strategy for flow cytometry analysis of Th1 and Th2 cells: CD11b$^-$F4/80$^-$ singlet cells are selected for double-positive CD45 and T cell receptor β (TCRβ) cells (R). Then, Th2 cells are defined as CD4$^+$IL-13$^+$ cells and Th1 cells as CD4$^+$IFNγ$^+$ cells (S).
(T and U) Proportion of Th2 (T) and Th1 cells (U) in the lungs of mice exposed or not exposed to silica microparticles and infected by *M. tuberculosis* H37Rv.
Representative of two independent experiments with similar results. Data are presented as means ± SEMs. In (B) n = 5 (−) and n = 4 (+ silica); (C)–(N) and (Q) n = 5 (−), n = 5 (+ silica), n = 4 (− H37Rv), and n = 5 (silica + H37Rv); (O) n = 3 (−), n = 5 (+ silica), n = 3 (− H37Rv) and n = 4 (silica + H37Rv); (T) and (U) n = 4 (− H37Rv) and n = 5 (silica + H37Rv) mice per group. Images are representative of four fields per mouse. Each point represents an individual mouse. *$p < 0.05$, **$p < 0.01$, ***$p < 0.001$, and ****$p < 0.0001$ (Student's t test for B, D, T, and U, or one-way ANOVA with Tukey's post hoc test). The correlation analyses were nonparametric (Spearman's correlation).

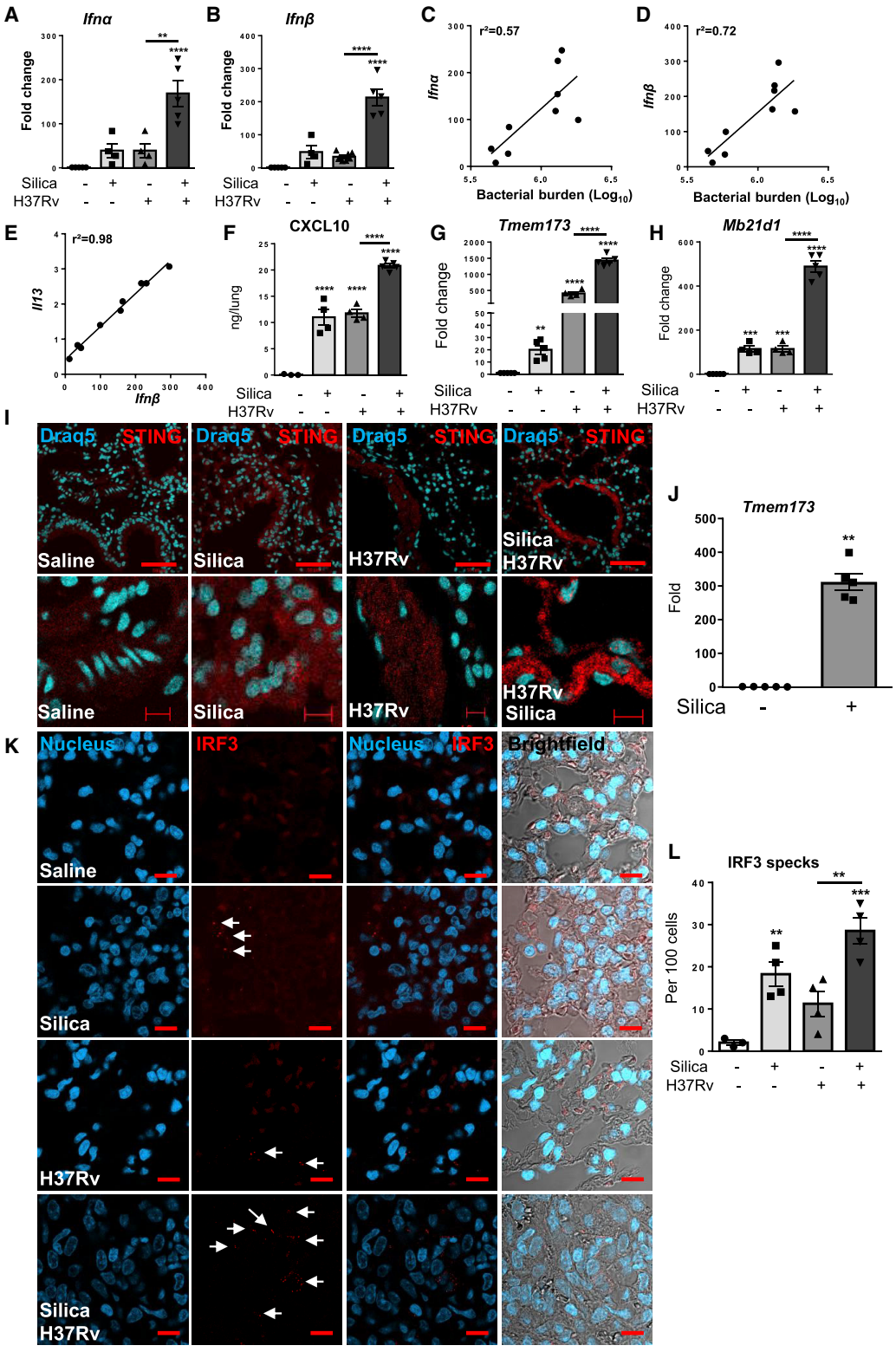


Figure 2. IFNI and STING Pathways Are Overexpressed in Silica Pre-exposed *M. tuberculosis*-Infected Mice

Silica microparticles (1 mg/mouse, i.t.) or saline vehicle was administered in WT mice 7 days before *M. tuberculosis* infection, as in Figure 1A. The parameters were analyzed in the lung on day 28 post-infection, unless otherwise indicated.

(A and B) mRNA levels of *Ifnα* (A) and *Ifnβ* (B) assessed by qRT-PCR.

(legend continued on next page)

Responses driven by the nucleic acid sensor cGAS/STING pathway are important for the induction of IFNI (Ablasser et al., 2013; Ishikawa and Barber, 2008; Ishikawa et al., 2009; Sun et al., 2013), and we next questioned the involvement of the cGAS/STING axis in silica-induced exacerbation of *M. tuberculosis* infection. Silica exposure triggered cell death and dsDNA release (Figures 1B and 1C), inducing the upregulation of STING-coding gene *Tmem173* (Figure 2G) and cGAS-coding gene *Mb21d1* (Figure 2H), which were also expressed after *M. tuberculosis* infection and further upregulated in the lungs of silica-pre-exposed *M. tuberculosis*-infected mice. Confocal microscopy revealed STING aggregates in the perinuclear region of silica-pre-exposed mice, less so in *M. tuberculosis*-infected mice, while STING aggregates were more prominent in the lungs of silica-pre-exposed *M. tuberculosis*-infected mice (Figure 2I). The STING-coding *Tmem173* gene was already strongly upregulated 7 days after silica exposure (Figure 2J), indicating that silica pre-exposure primed the host nucleic acid-sensing pathway, conditioning the host response to subsequent infection. IFN regulatory factor 3 (IRF3) speck formation was also increased in the lungs of mice co-challenged with silica pre-exposure and *M. tuberculosis* infection (Figures 2K and 2L). We present raised type 2 immunity and activation of cGAS/STING/IFNI pathways as a signature of silica-induced exacerbation of *M. tuberculosis* infection.

Extracellular DNA Induces Deleterious Type 2 Immunity after *M. tuberculosis* Infection

As DNA was released in the airways after silica exposure and/or *M. tuberculosis* infection, and the cGAS/STING pathway sensed dsDNA, we next tested the involvement of DNA in the host response to *M. tuberculosis* infection. To appreciate the contribution of extracellular DNA on the host immune response to *M. tuberculosis*, infected mice were treated with DNase I in conditions effectively degrading extracellular DNA (Figure 3A) (Benmerzoug et al., 2018; Toussaint et al., 2017). Both lung bacterial burden and *M. tuberculosis*-induced overall lung inflammation were reduced after systemic DNase I treatment (Figures 3B and 3C). We next questioned whether degrading extracellular dsDNA could affect the balance between type 1 and type 2 immunity. DNase I treatment increased IFNγ and IL-12p40 production after *M. tuberculosis* infection (Figures 3D and 3E). Conversely, *M. tuberculosis*-induced *Il4*, *Il13*, and to a lesser extent *Il5* genes were downregulated after DNase I treatment, demonstrating the crucial role of extracellular DNA in eliciting type 2 immunity after *M. tuberculosis* infection (Figures 3F–3H). Moreover, DNase I treatment reduced the proportion of Th2 cells seen in the lung after *M. tuberculosis* infection (Figures 3I–3K), while it increased the proportion of Th1 cells, as compared with *M. tuberculosis*-infected mice (Figures 3I, 3J, and 3L). Thus, extracellular DNA is key to promoting type 2 immunity favoring *M. tuberculosis* persistence, a response that can be abrogated by DNase I.

cGAS/STING Pathway Is Essential for Type 2 Immune Response in Silica-Induced Exacerbation of *M. tuberculosis* Infection

We next investigated the role of STING and cGAS in inducing type 2 immune responses after *in vivo* silica exposure plus *M. tuberculosis* infection, by co-challenging STING- and cGAS-deficient mice. The increased lung *M. tuberculosis* bacterial load, lung inflammation and inflammatory cell infiltration seen at 4 weeks of infection after silica pre-exposure in wild-type (WT) mice were absent in STING$^{-/-}$ and cGAS$^{-/-}$ mice (Figures 4A–4C), with no significant effect on bacterial dissemination to the spleen (Figure 4D). Furthermore, the reduction in IFNγ, IL-12p40 release, and *Nos2* gene expression seen after silica pre-exposure in *M. tuberculosis*-infected WT mice was abolished in STING$^{-/-}$ or cGAS$^{-/-}$ mice (Figures 4E–4G). Conversely, the exacerbation of type 2 immune response seen in the lung after silica exposure in *M. tuberculosis*-infected WT mice was abrogated in the absence of STING or cGAS, in terms of *Mrc1*, *Arg1*, *Il4*, *Il5*, and *Il13* gene expression (Figures 4H–4L) or MR staining (Figures 4M and 4N). Furthermore, the increase in Th2 cells induced by silica exposure in *M. tuberculosis*-infected WT mice was reduced in STING$^{-/-}$ and cGAS$^{-/-}$ mice (Figures 4O and 4P). However, the reduction in IFNγ-expressing Th1 cells in the co-challenged WT mice was prevented in the absence of STING or cGAS (Figures 4O and 4Q). The overexpression of *Ifn*α and *Ifn*β and higher production of CXCL10 observed after silica exposure and 4-week *M. tuberculosis* infection was significantly reduced in STING$^{-/-}$ and cGAS$^{-/-}$ mice, as was the formation of IRF3 punctate (Figure S1). Silica-induced type 2 immune response was persistent. At 8 weeks post-infection (Figure S2), silica pre-exposure yielded increased lung bacterial load and dissemination to the spleen, decreased type 1 marker *Nos2* but increased type 2 markers *Il4*, *Il5*, *Il13*, *Mrc1*, and *Chil3*, increased Th2 but decreased Th1 populations, and more prominent lung inflammation. These silica-induced parameters were prevented in STING$^{-/-}$ and cGAS$^{-/-}$ mice (Figure S2). These data provide direct evidence that the cGAS/STING pathway is essential for silica-induced exacerbation of *M. tuberculosis* infection by eliciting a deleterious type 2 immunity.

(C–E) Correlations between *Ifn*α and bacterial burden (C), *Ifn*β and bacterial burden (D), and *Il13* and *Ifn*β (E).
(F) ELISA measurement of CXCL10.
(G and H) mRNA levels of STING-related gene *Tmem173* (G) and cGAS-related gene *Mb21d1* (H).
(I) Confocal images of DNA dye Draq5 (blue) and STING specific antibody (red) staining. Bars, 50 μm; at higher magnification, 5μm.
(J) mRNA levels of STING-related gene *Tmem173* in the lung day 7 post-silica pre-exposure.
(K) Confocal images of DNA dye Draq5 (blue) and IRF3 (red) staining. Bars, 10 μm.
(L) Quantification of IRF3 specks per 100 cells.
Representative of two independent experiments with similar results are depicted. Data are presented as means ± SEMs. In (A)–(E) and (F)–(H) n = 3–5 (–), n = 4 (+ silica), n = 4 (– H37Rv), and n = 5 (silica + H37Rv); J, n = 5 (–) and n = 5 (+ silica); L, n = 4 (–), n = 4 (+ silica), n = 4 (– H37Rv), and n = 4 (silica + H37Rv) mice per group. Images are representative of four fields per mouse. Each point represents an individual mouse. *p < 0.05, **p < 0.01, ***p < 0.001, and ****p < 0.0001 (Student's t test for J, or one-way ANOVA with Tukey's post hoc test). The correlation analyses were nonparametric (Spearman's correlation).

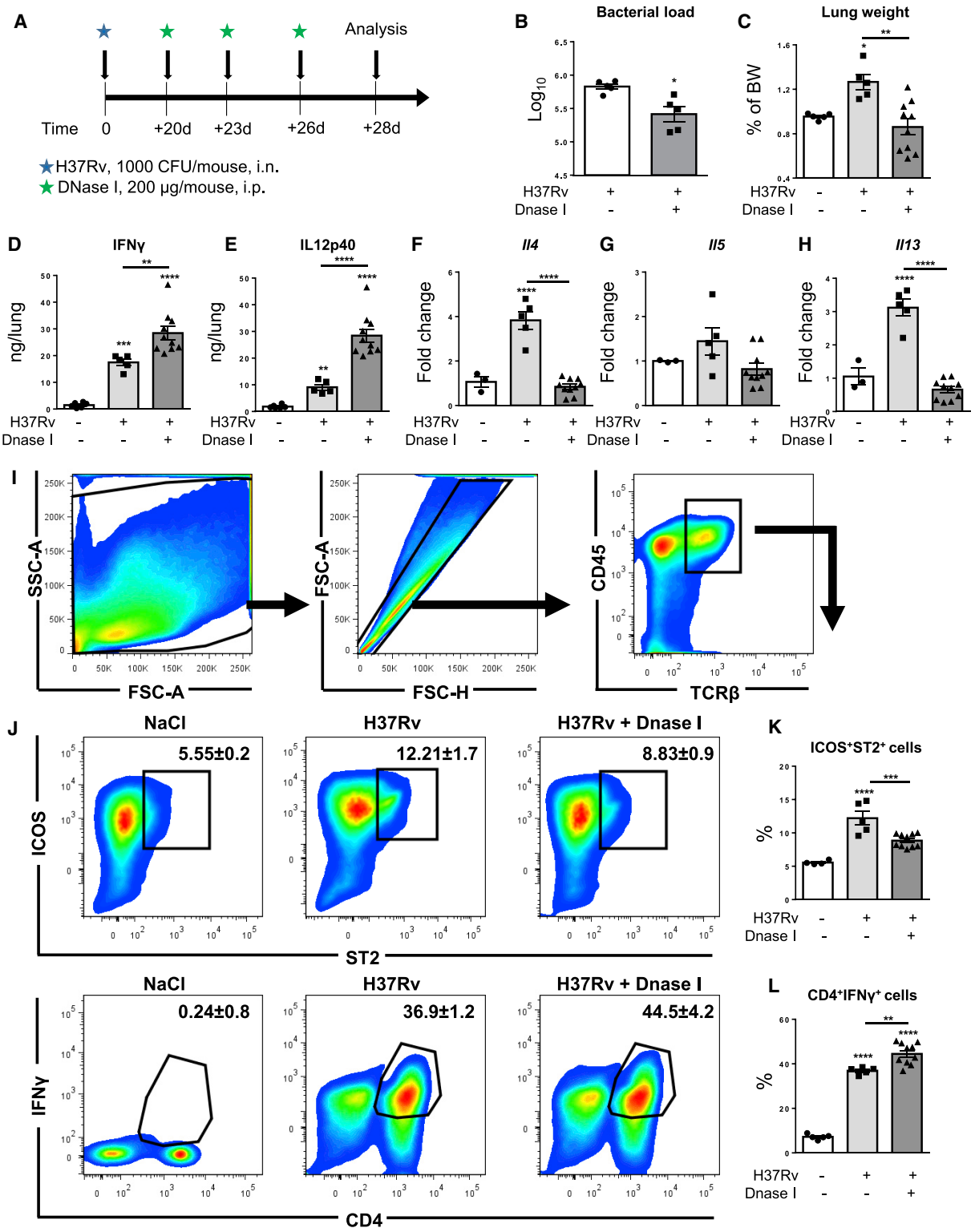


Figure 3. Extracellular DNA Is Central to Type 2 Immunity after *M. tuberculosis* Infection

(A) WT mice infected with *M. tuberculosis* H37Rv (1,000 CFUs/mouse, i.n.) received either DNase I (200 μg/mouse, i.p.) or vehicle control. The parameters were analyzed in the lung on day 28 post-infection.

(B) Bacterial burden.

(legend continued on next page)

Type 2 Immune Response in Silica-Induced Exacerbation of *M. tuberculosis* Infection Is Mediated by IFNI Signaling

To verify the contribution of IFNI signaling in inducing the type 2 immunity elicited after co-challenge by silica and *M. tuberculosis* infection, IFNα/β receptor (IFNAR)-deficient mice were exposed to silica and infected by *M. tuberculosis* (Figure S3). The overall lung inflammation evaluated by relative lung weight was increased in co-challenged WT mice, but not in IFNAR$^{-/-}$ mice (Figure S3A). The reduction in IL-12p40 and *Nos2* seen after silica exposure in *M. tuberculosis*-infected WT mice was absent in IFNAR$^{-/-}$ mice (Figures S3B and S3C). However, the overexpression of type 2-related genes *Mrc1*, *Arg1*, *Il4*, *Il5*, and *Il13* seen after silica exposure in *M. tuberculosis*-infected WT mice was abolished in IFNAR$^{-/-}$ mice (Figures S3D–S3H). Finally, the decrease in CD4^{+}IFNγ^{+} Th1 cells induced in co-challenged WT mice was absent in IFNAR$^{-/-}$ mice (Figures S3I and S3K), while the increase in CD4^{+}ST2^{+}ICOS^{+} Th2 cells after silica exposure of *M. tuberculosis*-infected WT mice was reduced in IFNAR$^{-/-}$ mice (Figures S3J and S3L). The increase in bacterial burden seen in WT mice pre-exposed to silica was absent in IFNAR$^{-/-}$ mice (Figure S3M), demonstrating the role of IFN in silica-induced *M. tuberculosis* infection exacerbation. Thus, silica-driven type 2 immunity after *M. tuberculosis* infection is induced through IFNI signaling.

Silica Pre-exposure Potentiates the Host Response to *M.tb* DNA to Induce Deleterious Type 2 Immune Responses

To address the mechanism by which silica pre-exposure exacerbates *M. tuberculosis* infection, we hypothesized that silica pre-exposure, inducing cell death and self-dsDNA release, may promote host cGAS/STING DNA sensing to respond to *M.tb* DNA. We thus questioned the role of *M.tb* DNA in the silica-induced exacerbation of *M. tuberculosis* infection. We investigated whether silica pre-exposure could potentiate the host response to *M.tb* DNA and recapitulate the features of silica-driven exacerbation of type 2 immune response seen after *M. tuberculosis* infection (Figure 5A). Silica exposure induced self-dsDNA release in the bronchoalveolar space, further raised after *M.tb* DNA administration (Figure 5B). *M.tb* DNA itself poorly influenced the type 1 immune response, even after silica pre-exposure, as seen with unaffected IL-12p40 and *Nos2* expression (Figures 5C and 5D). While *M.tb* DNA promoted some type 2 immune responses, they were exacerbated after silica pre-exposure, with a further 7- to 20-fold overexpression of *Arg1* and *Mrc1* genes (Figures 5E and 5F) and a further 5- to 10-fold upregulation of Th2-associated *Il4*-, *Il5*-, and *Il13*-coding genes in the lungs after silica pre-exposure plus *M.tb* DNA co-challenge (Figures 5G–5I). Silica exposure, or *M.tb* DNA alone, induced MR and IL-13 protein expression, which were overexpressed after silica pre-exposure plus *M.tb* DNA co-challenge (Figure 5J). However, iNOS protein expression was unaffected (Figure 5J). We next sought to identify whether M2 macrophages or Th2 cell populations were recruited to the lungs. Silica exposure plus *M.tb* DNA induced the pulmonary recruitment of F4/80^{+}CD206^{+} anti-inflammatory M2 macrophages and ICOS^{+}ST2^{+} Th2 cells (Figures 5K–5N). *M.tb* DNA administration after silica exposure also led to dendritic cell (DC) activation and eosinophilia (Figure S4). Thus, silica pre-exposure induces self-dsDNA release that upregulated the host DNA-sensing pathway to exacerbate host response to *M.tb* DNA, triggering a type 2 immune response with M2 and Th2 cell recruitment.

Silica Exposure Exacerbates the Activation of STING Pathway by *M.tb* DNA

We next examined the involvement of the STING pathway in silica pre-exposure-increased DNA-driven type 2 immunity. Silica pre-exposure induced the expression of STING (Figures 5O and 5P) and amplified the host response to *M.tb* DNA, leading to the aggregation of STING in the perinuclear region (Figure 5O). This recapitulated the raised STING expression seen in the lungs of mice infected with *M. tuberculosis* after silica exposure (Figure 2I). The downstream expression of *Ifnα* and *Ifnβ* genes and IFNI-induced CXCL10 was exacerbated after silica pre-exposure combined with *M.tb* DNA challenge (Figures 5Q–5S). Silica pre-exposure potentiated STING pathway activation by *M.tb* DNA, as seen by STING phosphorylation, dimerization, and phosphorylation of the TANK-binding kinase 1 (TBK-1) (Figure 5T). Thus, silica pre-exposure primed the host DNA-sensing STING pathway to full-blown activation and IFNI induction in response to *M.tb* DNA.

M.tb DNA Induces IFNI Response-Driven Type 2 Immunity

To address further the role of *M.tb* DNA in immune polarization *in vivo* in the absence of infection, heat-killed *M. tuberculosis* H37Rv (HKM.tb) was treated with DNase I (Figure S5A) and administered in the airways. We verified that DNase I effectively degraded *M.tb* DNA (Figure S5B). Administration of HKM.tb induced pulmonary *Ifn$\alpha\beta$* and CXCL10, which were reduced after DNase I treatment of HKM.tb, showing that *M. tuberculosis*-derived nucleic acids are essential to induce IFNI response *in vivo* (Figures S5C–S5E). HKM.tb induced IFNγ and IL-12p40 production, which was further increased by the DNase I treatment

(C) Relative lung weight.
(D and E) ELISA measurement of IFNγ (D) and IL-12p40 (E).
(F–H) mRNA levels of *Il4* (F), *Il5* (G), and *Il13* (H).
(I) Gating strategy for flow cytometry analysis in the lungs. Th1 and Th2 cells are pre-selected using CD11b^{-}F4/80^{-} singlet cells, followed by a selection of double-positive CD45 and TCRβ cells.
(J) Dot plots showing Th2 cells defined as ICOS^{+}ST2^{+} cells and Th1 cells as CD4^{+}IFNγ^{+} cells.
(K and L) Proportion of Th2 (K) and Th1 cells (L) in the lungs of infected WT mice receiving either DNase I or vehicle control.
Data are presented as means ± SEMs. In (B) n = 5 (H37Rv) and n = 5 (H37Rv + DNase I); (C)–(L) n = 3–5 (–), n = 5 (H37Rv), and n = 10 (H37Rv + DNase I) mice per group. Each point represents an individual mouse. *p < 0.05, **p < 0.01, ***p < 0.001, and ****p < 0.0001 (Student's t test for B, or one-way ANOVA with Tukey's post hoc test).

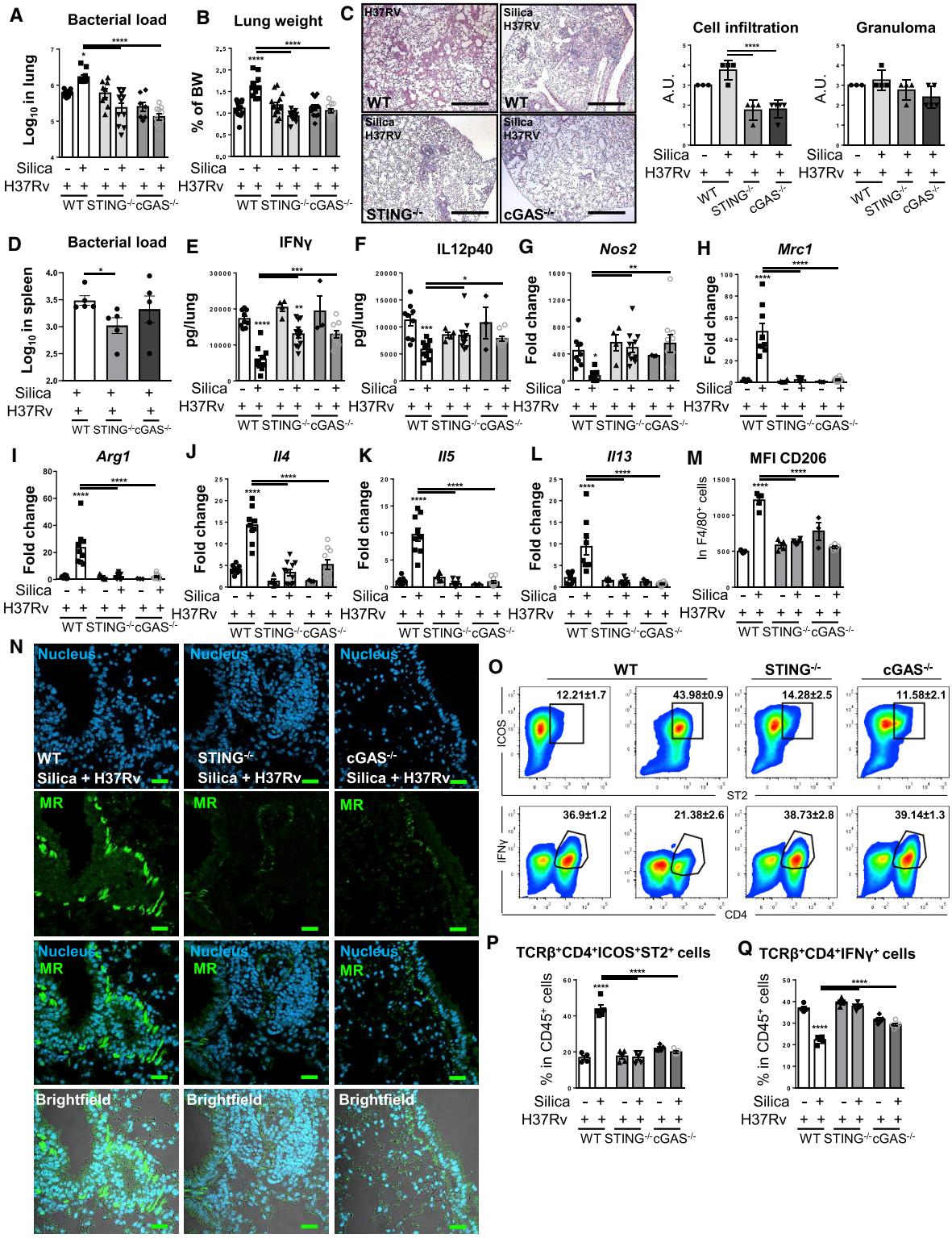


Figure 4. Silica-Induced Exacerbation of *M. tuberculosis* Infection Mediated by Type 2 Immune Response in a cGAS/STING-Dependent Manner

Silica microparticles (1 mg/mouse, i.t.) or saline vehicle was administered in WT, STING$^{-/-}$, and cGAS$^{-/-}$ mice until day 7 and then infected with *M. tuberculosis* H37Rv (1,000 CFU/mouse, i.n.), as shown in Figure 1A. The parameters were analyzed in the lung on day 28 post-infection, unless otherwise indicated.

(A) Lung bacterial burden.

(legend continued on next page)

(Figures S4G and S5F). *Nos2* expression was also upregulated by DNase I-treated HKM.tb (Figure S5H). Conversely, DNase I treatment reduced the expression of type 2-related *Mrc1*, *Il5*, and *Il13* genes induced by HKM.tb (Figures S5I–S5K). Furthermore, DNase I treatment of HKM.tb increased the proportion of Th1 cells (Figures S5L–S5N), while it decreased the proportion of Th2 cells recruited to the lung after HKM.tb exposure (Figures S5L, S5M, and S5O). Administration of *M.tb* DNA itself in the airways induced an IFNI inflammatory response, which was reduced by DNase I, while DNase I treatment alone had no effect (Figure S6). Thus, *M.tb* DNA plays a key role in dampening type 1 immune response and in polarizing type 2 immune response.

Silica Exposure and *M.tb* DNA Promote M2 Macrophage Polarization *In Vitro*

To further explore the mechanism underlying silica- and *M.tb* DNA-driven type 2 immunity, we investigated whether silica and *M.tb* DNA affect macrophage polarization *in vitro* (Figure 6A). Transfection of *M.tb* DNA had little influence on M1 macrophage markers such as IL-12p40 release and *Nos2* expression, as compared to controls stimulated with cyclic di-nucleotide AMP (cDN; Figures 6B and 6C). In contrast, pre-exposure to silica of macrophages transfected with *M.tb* DNA induced large amounts of IL-10 and overexpression of the M2 macrophage markers MR and arginase 1 coding genes (Figures 6D–6F). cDN alone did not induce the transcription of M2 markers *Mrc1* or *Arg1* (Figures 6E and 6F). The proportion of MR expressing $CD11c^{-}CD11b^{+}F4/80^{+}CD206^{+}$ macrophages was increased after silica exposure plus *M.tb* DNA transfection (Figures 6G–6I), with increased membrane MR expression as compared to either silica exposure or *M.tb* DNA transfection alone (Figures 6J and 6K). CD206 membrane expression was also exacerbated by silica plus cDN co-exposure, as compared to either cDN or silica alone (Figure S7), as was the expression of *Ym1* or *Ifnβ,* indicating that triggering STING through cDN, independently of cGAS, is enough to drive silica-induced type 2 reprogramming. The expression of MR was in line with STING activation, which was induced after silica exposure, and further increased after silica priming plus *M.tb* DNA transfection (Figure 6K). Silica pre-exposure induced macrophage cell death, and the co-challenge of silica plus *M.tb* DNA drastically increased cell death, as compared with *M.tb* DNA alone (Figures S8A and S8B). Cell death correlated with dsDNA release (Figures S8C and S8D) and with the overexpression of *Tmem173* and *Mb21d1* genes (Figures S8E and S8F). Thus, silica exposure triggers STING priming, which increases *M.tb* DNA-induced STING activation and macrophage switch toward an anti-inflammatory M2 phenotype *in vitro*.

STING Mediates the Switch toward M2 Macrophages in Response to Silica Plus *M.tb* DNA

As STING is activated *in vivo* and *in vitro* after silica priming and *M.tb* DNA challenge, we further examined the role of the cGAS/STING pathway in M2 macrophage polarization *in vitro*. We documented STING overexpression and aggregate formation in response to silica pre-exposure in WT and $cGAS^{-/-}$ macrophages, which was further increased after silica plus *M.tb* DNA in WT macrophages, but less so in $cGAS^{-/-}$ macrophages (Figure S9). The strong overexpression of CD206 and increased number of $CD11c^{-}CD11b^{+}F4/80^{+}CD206^{+}$ seen in WT macrophages after silica pre-exposure plus *M.tb* DNA transfection were abolished in the absence of STING in $STING^{-/-}$ macrophages (Figures 7A–7E). As STING activation in response to DNA requires an upstream DNA sensor, we addressed the involvement of cGAS as a DNA sensor. $cGAS^{-/-}$ macrophages displayed a reduced expression of CD206 and proportion of $CD11c^{-}CD11b^{+}F4/80^{+}CD206^{+}$ macrophages in response to silica pre-exposure plus *M.tb* DNA transfection, although this was less pronounced than for $STING^{-/-}$ macrophages (Figures 7A–7E). Silica pre-exposure abolished the induction of IL-12p40 or *Nos2* expression induced by *M.tb* DNA (Figures 7F and 7G). By contrast, silica pre-exposure primed macrophages to *M.tb* DNA, inducing an increase of IL-10 production and *Mrc1* expression in WT macrophages that was absent in STING- and cGAS-deficient macrophages (Figures 7H and 7I). Furthermore, confocal microscopy showed the overexpression of the MR CD206 in silica-exposed *M.tb* DNA transfected WT macrophages that was abrogated in $STING^{-/-}$ macrophages and less so in $cGAS^{-/-}$ macrophages (Figure 7J). This was accompanied by the activation of the IFNI response through STING and IRF3 pathways (Figure S10). Therefore, silica priming conditions macrophages to *M.tb* DNA-induced M2 polarization in a cGAS/STING-dependent manner.

(B) Relative lung weight.
(C) Lung tissue histology H&E staining, with pathology scoring of the presence of inflammatory cell infiltration and granuloma. Bars, 200 μm.
(D) Spleen bacterial burden.
(E and F) ELISA measurement of IFNγ (E) and IL-12p40 (F).
(G–L) mRNA levels of *Nos2* (G), *Mrc1* (H), *Arg1* (I), *Il4* (J), *Il5* (K), and *Il13* (L).
(M) MFI of MR CD206 expression in $CD45^{+}CD4^{-}$ $F4/80^{+}$ cells.
(N) Confocal images of DNA dye Draq5 (blue) and MR (green) staining. Bars, 50 μm.
(O) Flow cytometry analysis of lung Th1 and Th2 cells pre-gated using $CD11b^{-}F4/80^{-}$ singlet cells, followed by a selection of double-positive CD45 and TCRβ cells, as in Figure 1R. Th2 is defined as $ICOS^{+}ST2^{+}$ cells and Th1 as $CD4^{+}IFN\gamma^{+}$ cells.
(P and Q) Proportion of Th2 (P) and Th1 cells (Q) in the lungs of WT, $STING^{-/-}$, and $cGAS^{-/-}$ mice.
Representative of two independent experiments with similar results. Data are presented as means ± SEMs. In (A) n = 9–11 mice in all groups, except for 7 $cGAS^{-/-}$ H37Rv; (B) n = 10–14; (C) n = 3 (WT H37Rv), n = 4 (WT silica + H37Rv, $STING^{-/-}$ silica + H37Rv), and n = 5 ($cGAS^{-/-}$ silica + H37Rv); (D) n = 5; (E)–(L) n = 9 (WT H37Rv, WT silica + H37Rv), n = 4 ($STING^{-/-}$ H37Rv), n = 11 ($STING^{-/-}$ silica + H37Rv), n = 3 ($cGAS^{-/-}$ H37Rv), and n = 10 ($cGAS^{-/-}$ silica + H37Rv); (M) n = 5 (WT H37Rv, WT silica + H37Rv), n = 4 ($STING^{-/-}$ H37Rv), n = 6 ($STING^{-/-}$ silica + H37Rv), n = 3 ($cGAS^{-/-}$ H37Rv), and n = 5 ($cGAS^{-/-}$ silica + H37Rv); (P and Q) mice per group: n = 5 mice in all groups, except for 4 WT H37Rv. Images are representative of four fields per mouse. Each point represents an individual mouse. *p < 0.05, **p < 0.01, ***p < 0.001, and ****p < 0.0001 (one-way ANOVA with Tukey's post hoc test).
See also Figures S1, S2, and S3.

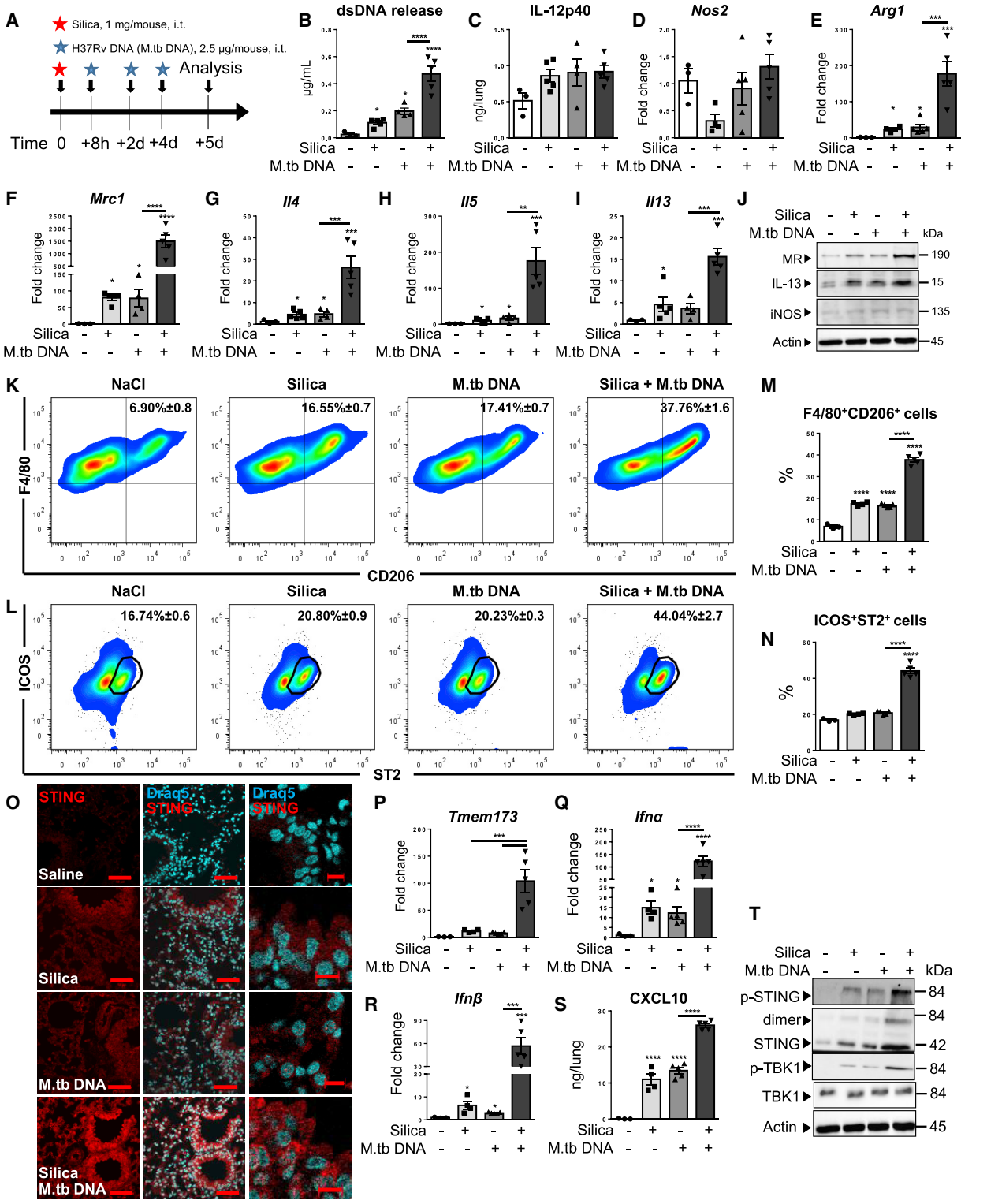


Figure 5. Silica Pre-exposure Plus *M.tb* DNA Induce Pulmonary Type 2 Immune Response

(A) Silica microparticles (1 mg/mouse, i.t.), DNA from *M. tuberculosis* H37Rv (*M.tb* DNA, 2,5 μg/mouse, i.t.), or saline vehicle was administered in WT mice. The parameters were analyzed on day 5 post-silica exposure.

(B) Concentration of extracellular dsDNA in the acellular fraction of BALF.

(legend continued on next page)

DISCUSSION

Silicosis is associated with an increased risk of developing pulmonary tuberculosis (Melo et al., 2016). The signals compromising the host response to *M. tuberculosis* infection in situations such as silica exposure remain poorly defined. Here, we investigated the mechanism underlying silica-induced exacerbation of *M. tuberculosis* infection. We show that pre-exposure to silica microparticles induces a dysregulation of type 1 versus type 2 immunity balance in favor of type 2 immune response after *M. tuberculosis* infection. Silica pre-exposure impairs the control of bacterial burden in the lungs of *M. tuberculosis*-infected mice. This is accompanied by an exacerbation of type 2 cytokines and cell recruitment, while type 1 immunity is reduced in terms of IFNγ, IL-12, NOS2, and Th1 recruitment to the lung. We hypothesized that by causing cell death and DNA release, silica pre-exposure primes the host immune response by triggering the cytosolic nucleic acid sensing pathway. DNA sensing is central to this response, as administration of *M.tb* DNA recapitulates the type 2/type 1 imbalance induced by silica pre-exposure, driving STING pathway activation and IFNI response. Conversely, DNase I treatment reversed the type 2 immune response induced by *M. tuberculosis*. STING and cGAS pathways are essential mediators of silica-induced type 2/type 1 imbalance after *M. tuberculosis* infection, as there was no exacerbation of infection in STING- or cGAS-deficient mice. Thus, our data show that silica pre-exposure triggers the cGAS/STING nucleic acid-sensing pathway that potentiates IFNI and type 2 immune responses to *M.tb* DNA, hampering the host control of *M. tuberculosis* infection.

M. tuberculosis has multiple ways to manipulate the host immune responses, and among these, induction of IFNI and IL-10 has been well documented (Moreira-Teixeira et al., 2018; O'Garra et al., 2013). STING and cGAS contribute to the *M. tuberculosis* induction of IFNI, detecting and binding to intracellular *M.tb* DNA (Collins et al., 2015; Manzanillo et al., 2012; Wassermann et al., 2015; Watson et al., 2015; Wiens and Ernst, 2016), a response that is further increased by *M.tb* RNA activation of the retinoic acid inducible gene-1 and mitochondrial antiviral-signaling protein (RIG-1 and MAVS)-dependent pathway (Cheng and Schorey, 2018). Here, we identified *M.tb* DNA as a signal for eliciting type 2 immunity, polarizing Th2 cells and anti-inflammatory M2 macrophages. *M.tb* DNA escapes from the bacilli and the phagosome through the ESAT-6 secretion system 1 (ESX-1) for inducing STING-driven IFNI response (Manzanillo et al., 2012; Wassermann et al., 2015). After internalization, *M. tuberculosis* induces programmed cell death, mainly through the production of the eicosanoids prostaglandin E_2 (PGE_2) and lipoxin A_4 (LXA_4) (Chen et al., 2008), leading to intracellular content spilling into the extracellular milieu, including host and *M.tb* DNA. To evaluate the impact of extracellular DNA from host or bacilli origin, a systemic treatment with DNase I was administered to *M. tuberculosis*-infected mice. Our results show that extracellular DNA plays an important role in the modulation of the immune system after *M. tuberculosis* infection, promoting type 2 immunity, which is detrimental to the host. The model used here, including silica pre-exposure for 7 days followed by 28 or 56 days of *M. tuberculosis* infection, may represent a smoldering, chronic exposure, as inflammatory parameters are usually reduced 5 weeks after silica, as compared to 1 or 7 days post-silica (Benmerzoug et al., 2018). Exposure to persistent microparticles such as silica, which induce cell death and release of extracellular DNA, primes the host nucleic acid sensing pathway, while further host DNA release may act as an adjuvant to amplify *M.tb* DNA-induced response.

The duality of the STING adaptor molecule, sensing nucleic acids from both the host and the pathogen, is central to explaining the exacerbated response to silica pre-exposure plus *M. tuberculosis* infection. STING is activated after *M. tuberculosis* infection *in vivo* (Collins et al., 2015; Marinho et al., 2018); however, silica pre-exposure induces STING expression and leads to the exacerbation of STING aggregation in the perinuclear region of host cells after *M. tuberculosis* infection. Administration of *M.tb* DNA *in vivo* leads to STING activation and recapitulates STING aggregation after silica pre-conditioning. *In vitro* in macrophages, silica exposure induced self-dsDNA release and STING aggregation, which was exacerbated by *M.tb* DNA. We show an interplay between the host response to silica, with self-dsDNA release, and the trigger of the STING pathway, which potentiates *M.tb* DNA sensing by STING and downstream responses.

How DNA can get access to the cytosol of host cells to activate STING is still a matter of debate. Cargo proteins can facilitate the transport of DNA into immune cells—among them, the antimicrobial peptide LL37, facilitating the transport

(C) ELISA measurement of IL-12p40 in the lungs.
(D–I) mRNA levels of *Nos2* (D), *Arg1* (E), *Mrc1* (F), *Il4* (G), *Il5* (H), and *Il13* (I) in the lungs.
(J) Immunoblots of MR, IL-13, iNOS, and β-actin as a reference in the lung homogenates.
(K and L) Gating strategy for flow cytometry analysis in the lungs. M2 macrophages and Th2 cell singlets are pre-selected using forward scatter area and forward scatter height (FSC-A/FSC-H), side scatter area and side scatter height (SSC-A/SSC-H), and forward scatter signal width and forward scatter area (FSC-W/FSC-A). For M2 macrophages, $CD11b^+$ cells are pre-gated, followed by a selection of double-positive F4/80 and CD206 cells (K). For Th2 cells, CD45 and TCRβ double-positive cells are pre-gated, followed by a selection of double-positive ICOS and ST2 cells (L).
(M and N) Proportion of M2 macrophages (M) and Th2 cells (N) in the lungs.
(O) Confocal images of DNA dye Draq5 (blue) and STING-specific antibody (red) staining in the lungs. Bars, 50 μm; at higher magnification, 5 μm.
(P–R) mRNA levels of *Tmem173* (P), *Ifnα* (Q), and *Ifnβ* (R) in the lungs.
(S) ELISA measurement of CXCL10 in the lungs.
(T) Immunoblots of phospho-STING, STING, phospho-TBK1, TBK1, and β-actin as a reference in the lung homogenates.
Data are presented as means ± SEMs, with n = 3 (–), n = 4–5 (silica), n = 4–5 (– H37Rv DNA), and n = 5 (silica + H37Rv DNA) mice per group. Images are representative of four fields per mouse. Each point represents an individual mouse. *$p < 0.05$, **$p < 0.01$, ***$p < 0.001$, and ****$p < 0.0001$ (one-way ANOVA with Tukey's post hoc test).
See also Figures S4, S5, and S6.

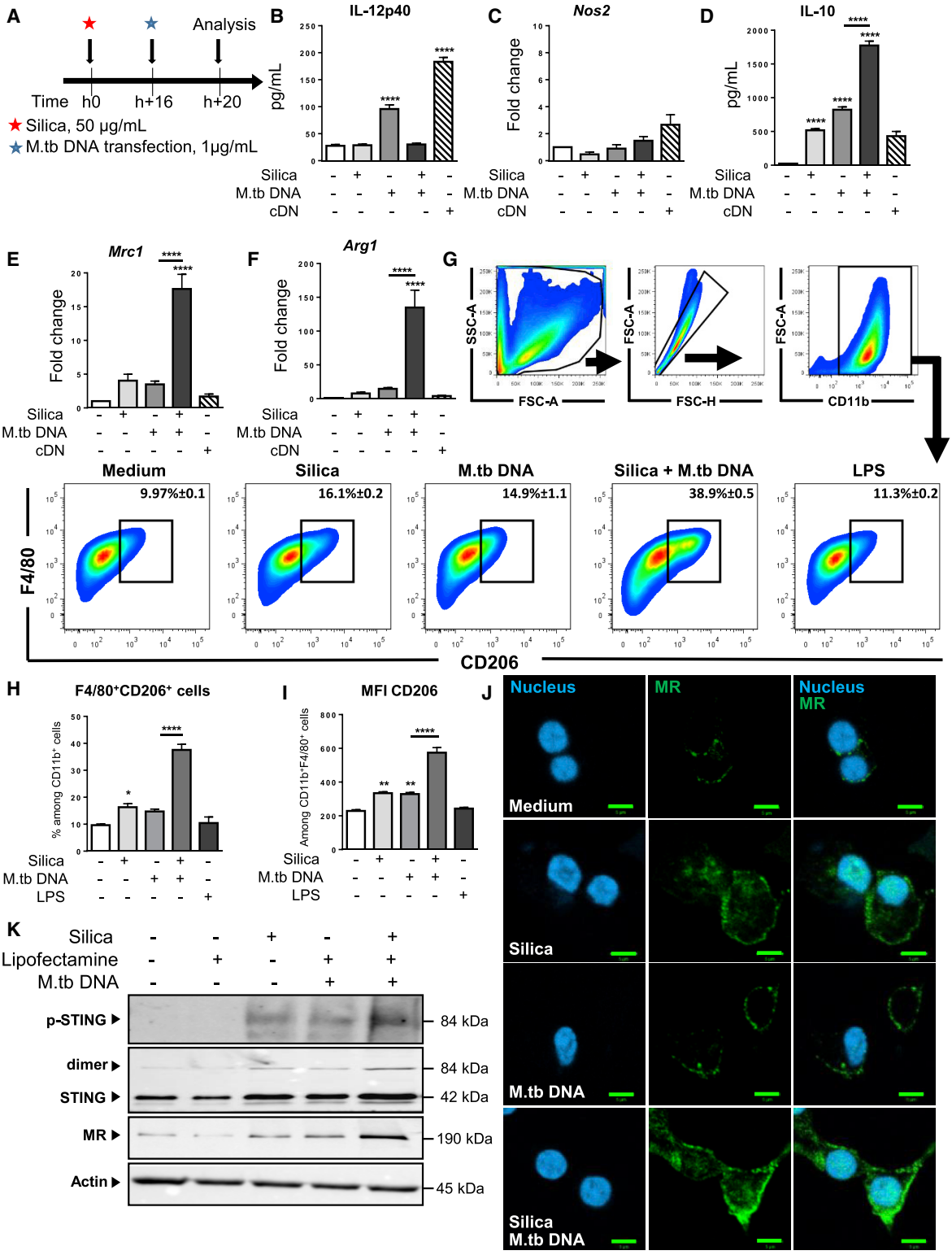


Figure 6. Silica and *M.tb* DNA Promote Anti-inflammatory M2 Macrophage Polarization *In Vitro*

(A–F) Bone marrow-derived macrophages from WT mice were stimulated with silica (50 μg/mL) for 16 h and then transfected with *M. tuberculosis* H37Rv DNA (1 μg/mL) for 4 h, as shown in (A). As a control for STING pathway activation, macrophages were transfected with the cyclic di-nucleotide AMP (cDN) for 4 h (6 μg/mL).

(legend continued on next page)

of self-dsDNA into antigen-presenting cells (Chamilos et al., 2012). Alternatively, after phagocytosis of apoptotic cells, DNA is normally degraded within lysosomes by DNase II, but undigested apoptotic cell-derived DNA could activate the cGAS/STING pathway (Blander, 2017). Membrane rupture of micronuclei formed in cells after mechanical or genotoxic stress also represents a way for the cGAS/STING pathway to access DNA (Mackenzie et al., 2017; Motwani and Fitzgerald, 2017).

Beyond the role of STING in nucleic acid sensing and induction of IFNI, we show here that the STING pathway can modulate the type 1 versus type 2 immune balance. The *in vivo* cytokine environment is crucial for inducing protective type 1 immunity after *M. tuberculosis* infection (O'Garra et al., 2013), elicited by macrophages, DCs, neutrophils and innate lymphoid cells (ILCs). In this study, we show that silica microparticles and *M.tb* DNA act in concert to polarize mature macrophages toward anti-inflammatory M2 macrophages. M2 macrophages are deleterious to the host, as they fail to eradicate *M. tuberculosis* bacilli (Huang et al., 2015, 2018). Overexpression of IL-1R–associated kinase M (IRAK-M), a negative regulator of Toll-like receptor (TLR) pathways, has been reported in the lungs of tuberculosis patients, and *in vitro* IRAK-M modulation is associated with the M2 phenotype and reduced *M. tuberculosis* control (Shen et al., 2017). M2 macrophages also secrete most type 2 cytokines such as IL-10, which inhibit type 1 cytokines TNFα, IFNγ, and IL-12. Here, we show that *M.tb* DNA drives M2 macrophages *in vitro* in a cGAS/STING-dependent manner. Self-dsDNA released after silica exposure *in vitro* induced STING and cGAS expression and activation, leading to the exacerbation of M2 polarization in *M.tb* DNA transfected macrophages via cGAS and STING. cDN recapitulated M2 polarization in silica-primed macrophages, indicating that triggering STING independently of cGAS drives silica-induced type 2 macrophage reprogramming.

IL-10 regulates innate and adaptive Th1 and Th2 responses (Huang et al., 2018). Released self-dsDNA from dying cells can directly stimulate CD4 T cells to induce Th2 cell differentiation and activation (Imanishi et al., 2014), but the role of *M.tb* DNA in this response was not investigated. Our *in vivo* studies also show that the cGAS/STING pathway contributes to generating Th2 cells and inhibiting Th1 cell expansion. This type 2 cytokine environment induced by self-dsDNA released after silica exposure plus *M.tb* DNA sensed by cGAS/STING reduces host resistance, which is beneficial for *M. tuberculosis* bacilli.

STING activation leads to IFNI response, and several studies reported a negative role for IFNI in host control after *M. tuberculosis* infection (Donovan et al., 2017; Dorhoi et al., 2014; Manca et al., 2001 , 2005; Moreira-Teixeira et al., 2018). Our data are in line with these observations, since IFNI response was increased and correlated with higher bacterial burden in the lungs of silica pre-exposed *M. tuberculosis*-infected mice. Furthermore, silica-induced exacerbation of *M. tuberculosis* infection was absent in IFNAR-deficient mice, indicating that IFNI is an integral part of this response. Type 2 immunity was reduced in the absence of IFNI signaling, whereas type 1 immunity was preserved. Thus, IFNI pathway activation in response to DNA sensing and STING activation is deleterious for the host by inducing type 2 immunity in silica-exposed *M. tuberculosis*-infected mice.

In conclusion, silica induced self-dsDNA release and trigger of STING pathway, which potentiated the cGAS/STING sensing of *M.tb* DNA, exacerbating downstream IFNI and type 2 immune response while dampening type 1 response to *M. tuberculosis* infection. Our findings identify an important role for nucleic acids derived from both the host and *M. tuberculosis* in a silica-induced exacerbation of *M. tuberculosis* infection. Controlling nucleic acid release or nucleic acid sensor activation may represent potential therapeutic options for the treatment of the silica-induced exacerbation of tuberculosis. This role for the STING pathway, at the crossroads of sterile inflammation and infection, goes beyond the implications of STING recognized in infection, cancer, autoimmunity, and, more recently, aging (Glück and Ablasser, 2019), indicating that the physiological activation of cGAS/STING pathway may condition the host response to infection.

STAR★METHODS

Detailed methods are provided in the online version of this paper and include the following:

- KEY RESOURCES TABLE
- CONTACT FOR REAGENT AND RESOURCE SHARING
- EXPERIMENTAL MODEL AND SUBJECT DETAILS
  - Mice
  - Bone marrow macrophages differentiation and stimulation
- METHOD DETAILS
  - *In vivo* animal experiments
  - Infection
  - *In vivo* DNase I treatment
  - Determination of cytokines and mediators
  - *M. tuberculosis* H37Rv DNA extraction and purification

(B and D) ELISA measurement of IL-12p40 (B) and IL-10 (D) in the cell supernatants.
(C, E, and F) mRNA levels of *Nos2* (C), *Mrc1* (E), and *Arg1* (F) were assessed by qRT-PCR on cell fraction.
(G–I) Macrophages were stimulated as in (A) or with lipopolysaccharide (LPS) (100 ng/mL) for 20 h, as a control of M1 macrophage polarization.
(G) Gating strategy for flow cytometry analysis. Macrophages singlets are pre-selected using FSC-A/FSC-H followed by a selection of CD11b$^+$ cells. Double positive F4/80 and CD206 M2 macrophages are gated. (H) Proportion of M2 macrophages.
(I) MFI of CD206$^+$ cells.
(J and K) Macrophages from WT mice were stimulated as in (A).
(J) Confocal images of DNA dye Draq5 (blue) and MR (green). Bars, 5 μm.
(K) Immunoblots of phospho-STING, STING, MR, and β-actin as a reference on macrophage cell fraction.
Representative of four independent experiments with similar results (A–I; n = 7 independent cultures for all conditions) or two independent experiments with similar results (J and K; n = 3 independent cultures for all conditions). Data are presented as means ± SEMs. Images are representative of four fields per independent culture and condition. *p < 0.05, **p < 0.01, and ****p < 0.0001 (one-way ANOVA with Tukey's post hoc test).
See also Figure S7.

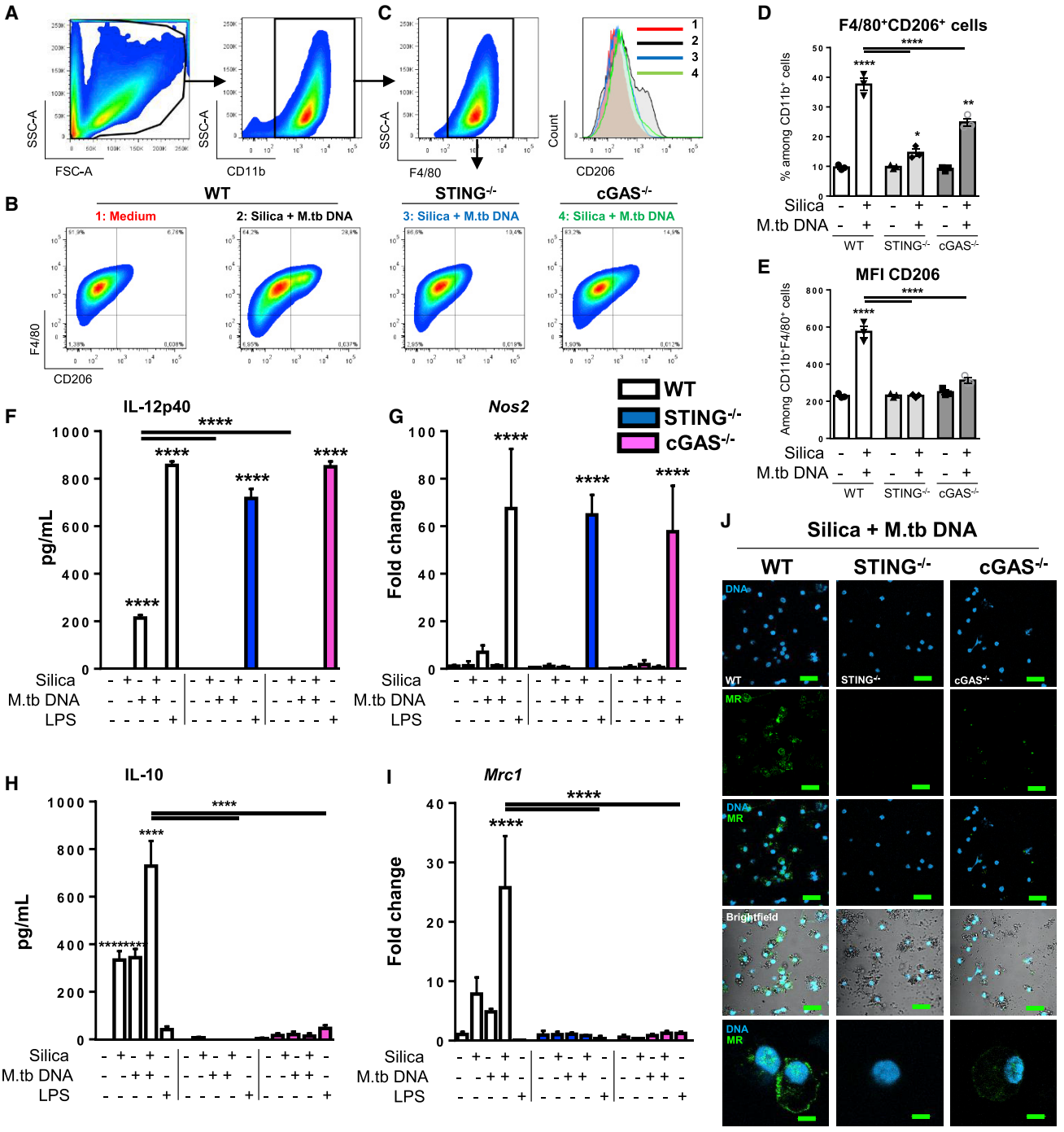


Figure 7. STING Pathway Plays a Key Role in M2 Macrophage Polarization in Response to Silica and *M.tb* DNA *In Vitro*

Bone marrow-derived macrophages from WT, STING$^{-/-}$ and cGAS$^{-/-}$ mice were stimulated with silica (50 μg/mL) for 16 h and then transfected with *M. tuberculosis* H37Rv DNA (1 μg/mL) for 4 h, as shown in Figure 6A. As a control of STING pathway activation, macrophages were transfected with the cDN for 4 h (6 μg/mL).

(A) Gating strategy for flow cytometry analysis. Macrophages singlets were pre-gated using FSC-A/FSC-H, followed by a selection of CD11b^{+} cells.

(B) Dot plots showing M2 macrophages defined as F4/80^{+}CD206^{+} cells.

(C) Dot plots showing macrophage-positive selection through CD11b^{+} and F4/80^{+} double staining, followed by histogram showing MFI of CD206. (1) Unstimulated WT macrophages, (2) WT macrophages exposed to silica and transfected with *M.tb* DNA, (3) STING$^{-/-}$ macrophages exposed to silica and transfected with *M.tb* DNA, and (4) cGAS$^{-/-}$ macrophages exposed to silica and transfected with *M.tb* DNA.

(D and E) Proportion of M2 macrophages (D) and MFI of CD206^{+} cells (E).

(legend continued on next page)

- Measurement of double-stranded DNA
- Quantitative RT-qPCR analysis
- Immunofluorescence microscopy
- Histopathological analysis
- Immunoblots
- Flow cytometry
- QUANTIFICATION AND STATISTICAL ANALYSIS
  - Statistical Analysis
- DATA AND SOFTWARE AVAILABILITY

SUPPLEMENTAL INFORMATION

Supplemental Information can be found online at https://doi.org/10.1016/j.celrep.2019.04.110.

ACKNOWLEDGMENTS

The authors thank Glen N. Barber for helpful discussions and sharing the STING-deficient mice, and Zhijian J. Chen for providing cGAS-deficient mice. This work was supported by the National Center for Scientific Research (CNRS), the University of Orléans, and European funding in Région Centre-Val de Loire (FEDER no. 2016-00110366 and EX005756′).

AUTHOR CONTRIBUTIONS

S.B. performed most of the experiments, with the assistance of B.B., S.R., D.G., A.X., N.R., and L.F. S.B., D.T., W.G.C.H., B.R., and V.F.J.Q. conceived the project, designed the experiments, and analyzed and interpreted the data. F.B., T.C., and L.F. provided resources and expertise. S.B., D.T., W.G.C.H., B.R., and V.F.J.Q. wrote the manuscript. All of the authors had the opportunity to discuss the results and comment on the manuscript.

DECLARATION OF INTERESTS

The authors declare no competing interests.

Received: December 5, 2018
Revised: March 17, 2019
Accepted: April 26, 2019
Published: May 28, 2019

REFERENCES

Ablasser, A., Goldeck, M., Cavlar, T., Deimling, T., Witte, G., Röhl, I., Hopfner, K.P., Ludwig, J., and Hornung, V. (2013). cGAS produces a 2′-5′-linked cyclic dinucleotide second messenger that activates STING. Nature *498*, 380–384.

Ahn, J., Gutman, D., Saijo, S., and Barber, G.N. (2012). STING manifests self DNA-dependent inflammatory disease. Proc. Natl. Acad. Sci. USA *109*, 19386–19391.

Barboza, C.E., Winter, D.H., Seiscento, M., Santos, Ude.P., and Terra Filho, M. (2008). Tuberculosis and silicosis: epidemiology, diagnosis and chemoprophylaxis. J. Bras. Pneumol. *34*, 959–966.

Benmerzoug, S., Rose, S., Bounab, B., Gosset, D., Duneau, L., Chenuet, P., Mollet, L., Le Bert, M., Lambers, C., Geleff, S., et al. (2018). STING-dependent sensing of self-DNA drives silica-induced lung inflammation. Nat. Commun. *9*, 5226.

Blander, J.M. (2017). The many ways tissue phagocytes respond to dying cells. Immunol. Rev. *277*, 158–173.

Calvert, G.M., Rice, F.L., Boiano, J.M., Sheehy, J.W., and Sanderson, W.T. (2003). Occupational silica exposure and risk of various diseases: an analysis using death certificates from 27 states of the United States. Occup. Environ. Med. *60*, 122–129.

Cambier, C.J., Takaki, K.K., Larson, R.P., Hernandez, R.E., Tobin, D.M., Urdahl, K.B., Cosma, C.L., and Ramakrishnan, L. (2014). Mycobacteria manipulate macrophage recruitment through coordinated use of membrane lipids. Nature *505*, 218–222.

Chamilos, G., Gregorio, J., Meller, S., Lande, R., Kontoyiannis, D.P., Modlin, R.L., and Gilliet, M. (2012). Cytosolic sensing of extracellular self-DNA transported into monocytes by the antimicrobial peptide LL37. Blood *120*, 3699–3707.

Chen, M., Divangahi, M., Gan, H., Shin, D.S., Hong, S., Lee, D.M., Serhan, C.N., Behar, S.M., and Remold, H.G. (2008). Lipid mediators in innate immunity against tuberculosis: opposing roles of PGE2 and LXA4 in the induction of macrophage death. J. Exp. Med. *205*, 2791–2801.

Cheng, Y., and Schorey, J.S. (2018). *Mycobacterium tuberculosis*-induced IFN-β production requires cytosolic DNA and RNA sensing pathways. J. Exp. Med. *215*, 2919–2935.

Cliff, J.M., Kaufmann, S.H., McShane, H., van Helden, P., and O'Garra, A. (2015). The human immune response to tuberculosis and its treatment: a view from the blood. Immunol. Rev. *264*, 88–102.

Collins, A.C., Cai, H., Li, T., Franco, L.H., Li, X.D., Nair, V.R., Scharn, C.R., Stamm, C.E., Levine, B., Chen, Z.J., and Shiloh, M.U. (2015). Cyclic GMP-AMP Synthase Is an Innate Immune DNA Sensor for Mycobacterium tuberculosis. Cell Host Microbe *17*, 820–828.

Cooper, A.M., Magram, J., Ferrante, J., and Orme, I.M. (1997). Interleukin 12 (IL-12) is crucial to the development of protective immunity in mice intravenously infected with mycobacterium tuberculosis. J. Exp. Med. *186*, 39–45.

Donovan, M.L., Schultz, T.E., Duke, T.J., and Blumenthal, A. (2017). Type I Interferons in the Pathogenesis of Tuberculosis: Molecular Drivers and Immunological Consequences. Front. Immunol. *8*, 1633.

Dorhoi, A., Yeremeev, V., Nouailles, G., Weiner, J., 3rd, Jörg, S., Heinemann, E., Oberbeck-Müller, D., Knaul, J.K., Vogelzang, A., Reece, S.T., et al. (2014). Type I IFN signaling triggers immunopathology in tuberculosis-susceptible mice by modulating lung phagocyte dynamics. Eur. J. Immunol. *44*, 2380–2393.

Flynn, J.L., Chan, J., Triebold, K.J., Dalton, D.K., Stewart, T.A., and Bloom, B.R. (1993). An essential role for interferon gamma in resistance to Mycobacterium tuberculosis infection. J. Exp. Med. *178*, 2249–2254.

Giordano, G., van den Brule, S., Lo Re, S., Triqueneaux, P., Uwambayinema, F., Yakoub, Y., Couillin, I., Ryffel, B., Michiels, T., Renauld, J.C., et al. (2010). Type I interferon signaling contributes to chronic inflammation in a murine model of silicosis. Toxicol. Sci. *116*, 682–692.

Glück, S., and Ablasser, A. (2019). Innate immunosensing of DNA in cellular senescence. Curr. Opin. Immunol. *56*, 31–36.

Hornung, V., Bauernfeind, F., Halle, A., Samstad, E.O., Kono, H., Rock, K.L., Fitzgerald, K.A., and Latz, E. (2008). Silica crystals and aluminum salts activate the NALP3 inflammasome through phagosomal destabilization. Nat. Immunol. *9*, 847–856.

(F and H) ELISA measurement of IL-12p40 (F) and IL-10 (H) in supernatant of WT, STING$^{-/-}$, and cGAS$^{-/-}$ macrophages.
(G and I) mRNA levels of *Nos2* (G) and *Mrc1* (I) were assessed by qRT-PCR on WT, STING$^{-/-}$, and cGAS$^{-/-}$ macrophages.
(J) Confocal images of DNA dye Draq5 (blue) and MR (green) staining on macrophages. Bars, 20 μm; at higher magnification, 5 μm.
Representative of three independent experiments with similar results (A–E; n = 3 independent cultures for all conditions), four independent experiments with similar results (F–I; n = 4 independent cultures for all conditions), or two independent experiments with similar results (J; n = 3 independent cultures for all conditions). Data are presented as means ± SEMs. Images are representative of four fields per independent culture and condition. Each point represents an individual mouse. ****p < 0.0001 (one-way ANOVA with Tukey's post hoc test).
See also Figures S8, S9, and S10.

Huang, Z., Luo, Q., Guo, Y., Chen, J., Xiong, G., Peng, Y., Ye, J., and Li, J. (2015). Mycobacterium tuberculosis-Induced Polarization of Human Macrophage Orchestrates the Formation and Development of Tuberculous Granulomas In Vitro. PLoS One *10*, e0129744.

Huang, L., Nazarova, E.V., Tan, S., Liu, Y., and Russell, D.G. (2018). Growth of *Mycobacterium tuberculosis* in vivo segregates with host macrophage metabolism and ontogeny. J. Exp. Med. *215*, 1135–1152.

Imanishi, T., Ishihara, C., Badr, Mel.S., Hashimoto-Tane, A., Kimura, Y., Kawai, T., Takeuchi, O., Ishii, K.J., Taniguchi, S., Noda, T., et al. (2014). Nucleic acid sensing by T cells initiates Th2 cell differentiation. Nat. Commun. *5*, 3566.

Ishikawa, H., and Barber, G.N. (2008). STING is an endoplasmic reticulum adaptor that facilitates innate immune signalling. Nature *455*, 674–678.

Ishikawa, H., Ma, Z., and Barber, G.N. (2009). STING regulates intracellular DNA-mediated, type I interferon-dependent innate immunity. Nature *461*, 788–792.

Joshi, G.N., and Knecht, D.A. (2013). Silica phagocytosis causes apoptosis and necrosis by different temporal and molecular pathways in alveolar macrophages. Apoptosis *18*, 271–285.

Konečný, P., Ehrlich, R., Gulumian, M., and Jacobs, M. (2019). Immunity to the Dual Threat of Silica Exposure and *Mycobacterium tuberculosis*. Front. Immunol. *9*, 3069.

Li, X.D., Wu, J., Gao, D., Wang, H., Sun, L., and Chen, Z.J. (2013). Pivotal roles of cGAS-cGAMP signaling in antiviral defense and immune adjuvant effects. Science *341*, 1390–1394.

Mackenzie, K.J., Carroll, P., Martin, C.A., Murina, O., Fluteau, A., Simpson, D.J., Olova, N., Sutcliffe, H., Rainger, J.K., Leitch, A., et al. (2017). cGAS surveillance of micronuclei links genome instability to innate immunity. Nature *548*, 461–465.

Manca, C., Tsenova, L., Bergtold, A., Freeman, S., Tovey, M., Musser, J.M., Barry, C.E., 3rd, Freedman, V.H., and Kaplan, G. (2001). Virulence of a Mycobacterium tuberculosis clinical isolate in mice is determined by failure to induce Th1 type immunity and is associated with induction of IFN-alpha /beta. Proc. Natl. Acad. Sci. USA *98*, 5752–5757.

Manca, C., Tsenova, L., Freeman, S., Barczak, A.K., Tovey, M., Murray, P.J., Barry, C., and Kaplan, G. (2005). Hypervirulent M. tuberculosis W/Beijing strains upregulate type I IFNs and increase expression of negative regulators of the Jak-Stat pathway. J. Interferon Cytokine Res. *25*, 694–701.

Manzanillo, P.S., Shiloh, M.U., Portnoy, D.A., and Cox, J.S. (2012). Mycobacterium tuberculosis activates the DNA-dependent cytosolic surveillance pathway within macrophages. Cell Host Microbe *11*, 469–480.

Marcy, C.H. (1950). Tuberculosis as a complication of silicosis. Pa. Med. J. *53*, 39.

Marinho, F.V., Benmerzoug, S., Oliveira, S.C., Ryffel, B., and Quesniaux, V.F.J. (2017). The Emerging Roles of STING in Bacterial Infections. Trends Microbiol. *25*, 906–918.

Marinho, F.V., Benmerzoug, S., Rose, S., Campos, P.C., Marques, J.T., Báfica, A., Barber, G., Ryffel, B., Oliveira, S.C., and Quesniaux, V.F.J. (2018). The cGAS/STING Pathway Is Important for Dendritic Cell Activation but Is Not Essential to Induce Protective Immunity against Mycobacterium tuberculosis Infection. J. Innate Immun. *10*, 239–252.

Mayer-Barber, K.D., Andrade, B.B., Oland, S.D., Amaral, E.P., Barber, D.L., Gonzales, J., Derrick, S.C., Shi, R., Kumar, N.P., Wei, W., et al. (2014). Host-directed therapy of tuberculosis based on interleukin-1 and type I interferon crosstalk. Nature *511*, 99–103.

McNab, F., Mayer-Barber, K., Sher, A., Wack, A., and O'Garra, A. (2015). Type I interferons in infectious disease. Nat. Rev. Immunol. *15*, 87–103.

Melo, V., Baia, L., Rita Gaio, A., and Duarte, R. (2016). Silicosis, tuberculosis time bomb? Rev. Port. Pneumol. (2006) *22*, 355–357.

Moreira-Teixeira, L., Mayer-Barber, K., Sher, A., and O'Garra, A. (2018). Type I interferons in tuberculosis: foe and occasionally friend. J. Exp. Med. *215*, 1273–1285.

Motwani, M., and Fitzgerald, K.A. (2017). cGAS Micro-Manages Genotoxic Stress. Immunity *47*, 616–617.

Müller, U., Steinhoff, U., Reis, L.F., Hemmi, S., Pavlovic, J., Zinkernagel, R.M., and Aguet, M. (1994). Functional role of type I and type II interferons in antiviral defense. Science *264*, 1918–1921.

O'Garra, A., Redford, P.S., McNab, F.W., Bloom, C.I., Wilkinson, R.J., and Berry, M.P. (2013). The immune response in tuberculosis. Annu. Rev. Immunol. *31*, 475–527.

Orme, I.M., Robinson, R.T., and Cooper, A.M. (2015). The balance between protective and pathogenic immune responses in the TB-infected lung. Nat. Immunol. *16*, 57–63.

Pfaffl, M.W., Horgan, G.W., and Dempfle, L. (2002). Relative expression software tool (REST) for group-wise comparison and statistical analysis of relative expression results in real-time PCR. Nucleic Acids Res. *30*, e36.

Popovic, I., Soares Magalhaes, R.J., Ge, E., Marks, G.B., Dong, G.H., Wei, X., and Knibbs, L.D. (2019). A systematic literature review and critical appraisal of epidemiological studies on outdoor air pollution and tuberculosis outcomes. Environ. Res. *170*, 33–45.

Porter, D.W., Hubbs, A.F., Mercer, R., Robinson, V.A., Ramsey, D., McLaurin, J., Khan, A., Battelli, L., Brumbaugh, K., Teass, A., et al. (2004). Progression of lung inflammation and damage in rats after cessation of silica inhalation. Toxicol. Sci. *79*, 370–380.

Porter, D.W., Millecchia, L.L., Willard, P., Robinson, V.A., Ramsey, D., McLaurin, J., Khan, A., Brumbaugh, K., Beighley, C.M., Teass, A., et al. (2006). Nitric oxide and reactive oxygen species production causes progressive damage in rats after cessation of silica inhalation. Toxicol. Sci. *90*, 188–197.

Quail, M.T. (2017). Overview of Silica-Related Clusters in the United States: Will Fracking Operations Become the Next Cluster? J. Environ. Health *79*, 20–27.

Schreiber, T., Ehlers, S., Heitmann, L., Rausch, A., Mages, J., Murray, P.J., Lang, R., and Hölscher, C. (2009). Autocrine IL-10 induces hallmarks of alternative activation in macrophages and suppresses antituberculosis effector mechanisms without compromising T cell immunity. J. Immunol. *183*, 1301–1312.

Shen, P., Li, Q., Ma, J., Tian, M., Hong, F., Zhai, X., Li, J., Huang, H., and Shi, C. (2017). IRAK-M alters the polarity of macrophages to facilitate the survival of Mycobacterium tuberculosis. BMC Microbiol. *17*, 185.

Srivastava, S., Ernst, J.D., and Desvignes, L. (2014). Beyond macrophages: the diversity of mononuclear cells in tuberculosis. Immunol. Rev. *262*, 179–192.

Sun, L., Wu, J., Du, F., Chen, X., and Chen, Z.J. (2013). Cyclic GMP-AMP synthase is a cytosolic DNA sensor that activates the type I interferon pathway. Science *339*, 786–791.

Toussaint, M., Jackson, D.J., Swieboda, D., Guedán, A., Tsourouktsoglou, T.D., Ching, Y.M., Radermecker, C., Makrinioti, H., Aniscenko, J., Bartlett, N.W., et al. (2017). Host DNA released by NETosis promotes rhinovirus-induced type-2 allergic asthma exacerbation. Nat. Med. *23*, 681–691.

Wassermann, R., Gulen, M.F., Sala, C., Perin, S.G., Lou, Y., Rybniker, J., Schmid-Burgk, J.L., Schmidt, T., Hornung, V., Cole, S.T., and Ablasser, A. (2015). Mycobacterium tuberculosis Differentially Activates cGAS- and Inflammasome-Dependent Intracellular Immune Responses through ESX-1. Cell Host Microbe *17*, 799–810.

Watson, R.O., Bell, S.L., MacDuff, D.A., Kimmey, J.M., Diner, E.J., Olivas, J., Vance, R.E., Stallings, C.L., Virgin, H.W., and Cox, J.S. (2015). The Cytosolic Sensor cGAS Detects Mycobacterium tuberculosis DNA to Induce Type I Interferons and Activate Autophagy. Cell Host Microbe *17*, 811–819.

Wiens, K.E., and Ernst, J.D. (2016). The Mechanism for Type I Interferon Induction by Mycobacterium tuberculosis is Bacterial Strain-Dependent. PLoS Pathog. *12*, e1005809.

STAR★METHODS

KEY RESOURCES TABLE

REAGENT or RESOURCE	SOURCE	IDENTIFIER
Antibodies		
CD16/CD32	BD biosciences	2.4G2
IA/IE-BV785	BD biosciences	M5/114
TCRβ chain-APC-Cy7	BD biosciences	H57-597
CD11b-BV421	BD biosciences	M1/70
CD45-A700	BD biosciences	30-F11
F4/80-PE-Cy7	BD biosciences	BM8
IL-13-eF660	eBioscience	eBio13A
IFNγ-PE	Biolegend	XMG1.2
CD4-APC	BD biosciences	RM4-5
CD8α-FITC	BD biosciences	53-6.7
ICOS-BV421	Biolegend	C398.4A
ST2-PE-Cy7	Biolegend	DIH4
CD206-APC	Biolegend	C068C2
CD170-PE	Biolegend	S17007L
FITC Annexin V Apoptosis Detection Kit I	BD biosciences	556547
Goat anti-Rabbit IgG (H+L) Cross-Adsorbed, Alexa Fluor 532, Polyclonal, Secondary Antibody	Fisher scientific	A11009
Rabbit polyclonal to Tmem173	Abcam	ab92605
Phospho-STING (Ser366) Rabbit mAb	Cell Signaling	D7C3S
Rabbit polyclonal to IRF3	Cell Signaling	D83B9
Rabbit anti-TBK1/NAK	Cell Signaling	D1B4
Rabbit anti-Phospho-TBK1/NAK (Ser172)	Cell Signaling	D52C2
Rabbit anti-Phospho-IRF-3 (Ser396)	Cell Signaling	4D4G
Anti-Mannose Receptor antibody	Abcam	ab64693
Anti-iNOS antibody	Abcam	ab3523
Anti-IL-13 antibody	Abcam	ab109815
Anti-alpha smooth muscle Actin	Abcam	ab21027
Bacterial and Virus Strains		
M. tuberculosis H37Rv	This manuscript	N/A
Biological Samples		
Lung	This manuscript	N/A
Spleen	This manuscript	N/A
Bronchoalveolar lavage fluid	This manuscript	N/A
Bonne marrows	This manuscript	N/A
Chemicals, Peptides, and Recombinant Proteins		
DNase I	Sigma	DN25-1G
Liberase	Sigma	5 401 127 001
Trizol	Sigma	15596026
Crystalline silica	DMT	N/A
Lipofectamine 2000	Thermofisher	11 668 027
Critical Commercial Assays		
GoScript Reverse Transcription System	Promega	A5001
GoTaq® qPCR Master Mix	Promega	A6002

(*Continued on next page*)

Continued		
REAGENT or RESOURCE	SOURCE	IDENTIFIER
Quant-iT PicoGreen dsDNA	ThermoFisher	P11496
Mouse IL-12/IL-23 p40 Allele-specific DuoSet ELISA	R&D systems	DY499
Duoset ELISA IP-10	R&D systems	DY466
Mouse IL-10 DuoSet ELISA	R&D systems	DY417
Mouse IFN-gamma DuoSet ELISA	R&D systems	DY485
DC Protein assay kit	Bio-Rad	5000111
Experimental Models: Cell Lines		
Bone marrow derived macrophages	This manuscript	N/A
Experimental Models: Organisms/Strains		
Mouse C57BL/6 STING$^{-/-}$	Ahn et al., 2012	N/A
Mouse C57BL/6 cGAS$^{-/-}$	Li et al., 2013	N/A
Mouse C57BL/6 IFNAR$^{-/-}$	Müller et al., 1994	N/A
Mouse C57BL6 IRF3$^{-/-}$	RIKEN BRC	RBRC00858
Oligonucleotides		
M. tuberculosis H37Rv DNA	This manuscript	N/A
Cyclic di-adenylate monophosphate, c-di-AMP	Invivogen	tlrl-nacda
See also Table S1		N/A
Software and Algorithms		
Graphpad Prism 6	Graphpad Software, San Diego, USA	https://www.graphpad.com/
Bio-Plex Manager software	Bio-Rad	Bio-rad, Bio-Plex Manager
FlowJo software	TreeStar, Mountain View, CA	https://www.flowjo.com
Carl Zeiss Vision Viewer 4.8	Carl Zeiss	Carl Zeiss
Zeiss LSM Image Browser	Carl Zeiss	Carl Zeiss

CONTACT FOR REAGENT AND RESOURCE SHARING

Further information and requests for resources and reagents should be directed to and will be fulfilled by the Lead Contact, Valerie Quesniaux (quesniaux@cnrs-orleans.fr).

EXPERIMENTAL MODEL AND SUBJECT DETAILS

Mice

Wild-type (WT) C57BL/6 mice and mice deficient for STING (STING$^{-/-}$) (Ahn et al., 2012), cGAS (cGAS$^{-/-}$) (Li et al., 2013), IFNAR (IFNAR$^{-/-}$) (Müller et al., 1994), or IRF3 (IRF3−/−, RIKEN RBRC00858) were bred in our specific pathogen free animal facility at CNRS (TAAM UPS44, Orleans, France). For experiments, gender-matched adult (8-12 week old) animals were maintained in ventilated cages or, for the infectious protocols, in biological isolation safety cabinet glove boxes in a biohazard animal unit, in a temperature-controlled (23°C) facility with a strict 12 h light/dark cycle with food and water provided *ad libitum*, and monitored daily. All animal experiments complied with the French Government's animal experiment regulations and were approved by the ''Ethics Committee for Animal Experimentation of CNRS Campus Orleans'' (CCO) under number CLE CCO 2015-1071.

Bone marrow macrophages differentiation and stimulation

Bone-marrow-derived macrophages (BMDMs) were generated by differentiating mouse bone marrow cells for 7 days in DMEM medium (GIBCO, Life Technologies) supplemented with 10% FCS (GIBCO, Life Technologies), 100U/mL penicillin and 100μg/mL streptomycin (GIBCO), 2mM glutamine (Sigma-Aldrich), plus 20% horse serum and 30% (v/v) L929 conditioned medium as a source of M-CSF. After washing and re-culturing for 3 days in fresh medium, BMDMs were pre-stimulated during 16hrs with silica microparticles (50 μg/mL) or unstimulated. Then, cells were washed and transfected during 4hrs with *M. tuberculosis* H37Rv DNA (1μg/mL) or the cyclic di-nucleotide (cDN) c-di-AMP (6 μg/mL), or unstimulated. Nucleic acids were transfected using Lipofectamine 2000.

Particles

Crystalline silica particles (DQ12, d_{50} = 2,2μm, DMT GmbH and Co. KG, Essen, Germany) were sterilized by heating at 200°c for 4 hr (Giordano et al., 2010). The freshly prepared suspension was autoclaved at 121°C for 30 min before use.

METHOD DETAILS

In vivo animal experiments

Silica airway exposure

Crystalline silica particles (1mg/mouse in 0.9% saline) or saline vehicle was administered intratracheally (i.t.) to mice under isoflurane anesthesia, one week prior to *M. tuberculosis* infection. Bronchoalveolar lavage (BAL) was performed by washing the lungs four times with 0.5 mL of saline solution at room temperature. After centrifugation at 400 x g for 10 min at 4°C, the cells were counted. The supernatant of the first lavage was collected after centrifugation and stored at −80°C for dsDNA quantification (Quant-iT PicoGreen).

Infection

Aliquots of *M. tuberculosis* H37Rv kept frozen at −80°C were thawed, diluted in sterile saline containing 0.05% Tween 20 and clumping disrupted by 50 repeated aspirations through 18, 20, 26, 27 and 30 gauge needles (Omnican, Braun, Germany). Pulmonary infection with *M. tuberculosis* H37Rv was performed by delivering 1000 ± 150 CFU/mouse into the nasal cavities under light ketamine (100mg/kg)-xylasine (10mg/kg) anesthesia. The bacterial load in the lungs was determined on day 1 post infection in control mice. For quantifying bacterial burden at days 28 and 56 post-infection, lungs and spleens were weighted, defined aliquots homogenized in phosphate-buffered saline (PBS; Dispomix homogenizer, Medic Tools, Switzerland), and tenfold serial dilutions prepared in 0.05% Tween 20 containing 0.9% NaCl were plated in duplicates onto Middlebrook 7H11 (Difco) agar plates containing 10% OADC. After 3 weeks incubation at 37°C colonies were enumerated, and results expressed as $\log_{10}$ CFU per organ.

In vivo DNase I treatment

Mice were treated with extracellular DNase I (Sigma®; 200μg/mouse, i.p.) 20, 23 and 26 days after *M. tuberculosis* H37Rv infection or 4hrs before and 8hrs after administration of DNA from *M. tuberculosis* H37Rv (M.tb DNA; 2.5 μg/mouse, i.t.).

Determination of cytokines and mediators

TNFα, IFNγ, IL-12p40, CXCL10 and IL-10 protein concentration in lung homogenate or cell culture supernatants were quantified by enzyme-linked immunosorbent assay (ELISA; R&D Duoset, Systems, Abingdon, UK) following the manufacturer's instructions. Lung homogenates were centrifuged (3 min at 14,500 rpm), the supernatants sterilized by centrifugation through 0.45μm and 0.22 μm filters (3 min at 14,500 rpm; Costar-Corning, Badhoevedorp, the Netherlands), were immediately frozen on dry ice and stored at −80°C until cytokine content determination.

M. tuberculosis H37Rv DNA extraction and purification

Mycobacteria were grown to late log phase in Middlebrook 7H9 medium (10 mL) and harvested by centrifugation at 6,000 x g for 10 min. The pellet was resuspended in 10 mL of TE buffer (10 mM Tris-HCl [pH 8.0], 1 mM EDTA) and centrifuged again at 6,000 x g for 10 min. The semidried mycobacterial pellet was resuspended into 1 mL TE buffer (10 mM Tris-HCl [pH 8.0], 1 mM EDTA). After the addition of 100 μl of lysozyme (200 mg/mL) and incubation overnight at 37°C, 100 μL of SDS 10% and 50 μL Proteinase K (20 mg/mL) (Macherey-Nagel) were added and incubated 4 h at 56°C. 100 μL of 10% CTAB were mixed and incubated for 1 h at 65°C. One volume of phenol-chloroform-isoamyl alcohol (25:24:1 (vol/vol)) was added and the solution was vigorously mixed and then centrifuged at 14,000 x g for 5 min in phase lock gel (QIAGEN). The supernatant was mixed with 1 volume of chloroform-isoamyl alcohol (24:1 (vol/vol)) and centrifuged again. The DNA was precipitated by the addition of 0.8 volume of isopropanol and 0.3 M sodium acetate (final concentration). After centrifugation for 30 min at 14,000 x g, the DNA was air-dried, dissolved in 50 μL of Tris buffer (5 mM Tris-HCl [pH 8.5]) and stored at −20°C until further use.

Measurement of double-stranded DNA

dsDNA was measured in the BALF using Quant-iT PicoGreen dsDNA reagent (Invitrogen, Carlsbad, CA), according to the manufacturer's protocol. For dsDNA measurement using Quant-iT PicoGreen dsDNA reagent in cell supernatant, cells were stimulated in a DMEM high glucose without phenol red medium (ThermoFisher Scientific, Waltham, USA).

Quantitative RT-qPCR analysis

Total RNA was collected and extracted in TRI-Reagent (Sigma). RNA integrity and quality was controlled using Agilent RNA 6000 Nanopuces kit®. Reverse transcription was performed with SuperScript®III Kit (Invitrogen) and cDNA was subjected to quantitative real-time PCR using primers for *Ifnα4*, *Ifnβ1*, *Tmem173, Mb21d1, Il4, Il5, Il13, Nos2, Mrc1, Ym1 (Chil3)* and *Arg1* (QIAGEN) and GoTaq® qPCR-Master Mix (Promega). RNA expression was normalized to *Gapdh* expression (QIAGEN). Data were analyzed using the comparative analysis of relative expression, by $^{\Delta\Delta}$Ct methods (Pfaffl et al., 2002).

Immunofluorescence microscopy

Lung tissue frozen in OCT, 10 μm lung sections were performed by cryostat (Leica®) and heated at 80°C for 40min in citrate 10mM pH = 6. Lung cells were permeabilized with 0.5% Triton X-100 in 2% BSA in PBS-FCS (v/v) 10% for 1 hr, washed three times in PBS

and incubated overnight with rabbit anti-STING (ab92605 1/50, Abcam) or with rabbit anti-IRF3 (D83B9 1/100, Cell Signaling) in PBS containing 2% BSA, 10% FCS and 0,5% Triton X-100. The lung sections were washed with PBS and incubated with anti-rabbit IgG Alexa 532 secondary antibody (1/100) for 1 hr. Following washing, cells were stained with DNA dye Draq5 (1/1000) for 15 min, washed with PBS, and mounted onto microscope slides (Fluoromount). Cells were observed by using a Zeiss Axiovert 200M microscope coupled with a Zeiss LSM 510 Meta scanning device (Carl Zeiss Co. Ltd.,Iena, Germany). The inverted microscope was equipped with a Plan-Apochromat 63X objective (NA = 1.4) Images were acquired using Zeiss LSM Image Browser (Carl Zeiss Co. Ltd.,Iena, Germany). At least 4 sections for each animal per experimental group were selected for image analysis of IRF3 specks using the thresholding technique after subtraction of background. The quantifications were done by counting ca 300 cells in 4 separated lung regions (BD LSM Image Browser Software).

In vitro cultured BMDMs were harvested, washed twice in cold-PBS and plated on coverslips overnight at 37°C 5% CO_2 in DMEM complemented with 5% (v/v) FCS. After stimulation, BMDMs were fixed with 4% paraformaldehyde in PBS for 15 min, permeabilized with 0.2% Triton X-100, blocked with 3% BSA in PBS for 30 min, and incubated overnight with rabbit anti-mannose receptor (ab64693, 1/50, Abcam) containing 1% BSA and 0.1% Triton X-100 in PBS at room temperature (RT). Cells were washed with PBS and incubated with anti-rabbit IgG Alexa 532 fluorescence secondary antibody (1/100) for 1 hr at RT. After washing, cells were stained with DNA dye Draq5 (1/1000) for 3 min, washed with PBS, and mounted onto microscope slides and images acquired as above.

Histopathological analysis

Lung tissues were fixed in 4% buffered formaldehyde overnight, paraffin-embedded, and 3 μm sections were stained with hematoxylin and eosin (HE). Histologic changes were determined by using a semiquantitative severity score (0-5) for inflammatory cell infiltration and granuloma (0-5). The slides were examined blindly with a Nikon microscope (Nikon eclipse 80i; Nikon, Tokyo, Japan).

Immunoblots

Lung tissue or BMDMs were lysed with 0.5 mL of 1X RIPA lysis buffer (50 mM Tris pH 7.5, 150 mM sodium chloride, 0.5% sodium deoxycholate, and 1% NP-40) containing 1X complete EDTA-free Protease inhibitor cocktail tablets (Roche Diagnostics), 1X Phosphatase Inhibitor Cocktail 2 (Sigma-Aldrich), 1 mM sodium orthovanadate (Sigma-Aldrich), 25 mM sodium fluoride (Sigma-Aldich), and 1 mM phenylmethylsulfonyl fluoride (Sigma-Aldrich). The lysates were centrifuged and protein concentration was quantified in the supernatant by using DC Protein Assay Kit (Bio-Rad®). Total protein (30 μg) was loaded per sample on 8% polyacrylamide gel and run at 160V for 45 min using the Bio-Rad Mini-PROTEAN Tetra Cell. Proteins were transferred from the gel to a nitrocellulose membrane using a Trans-Blot SD. Transfer System; Bio-Rad at 100V for 45 min. Successful protein transfer was confirmed by using Ponceau S staining (Sigma-Aldrich). Membranes were blocked with 10% non-fat milk in 1X TBS-T (20 mM Tris Base, 150 mM sodium chloride, and 0.05% Tween-20 pH 7.6). Primary antibodies used were from rabbit anti-STING (#ab92605; Abcam) and mouse anti-mouse beta actin (#ab8226; Abcam). Antibodies were used according to the manufacturer's instructions. Portions of the membrane were incubated 2 hr at RT in 5% non-fat milk in TBS-T at the appropriate dilutions, then washed in TBS-T three times for 10 min each at room temperature. Membranes were incubated with goat anti-rabbit-IgG-HRP-conjugated or mouse anti-mouse-IgG-HRP-conjugated secondary antibodies (Bio-Rad) diluted in 5% non-fat milk in TBS-T for 1 hr at RT. The membranes were washed three times in TBS-T and Amersham ECL Prime Western Blotting Detection Reagent (Thermofischer) was used to develop the blots on film (PXi gel doc system®).

Flow cytometry

The left lung lobe was harvested and lung cells were isolated by enzymatic digestion using liberase (125 μg/mL; Roche) and DNase I (1 mg/mL; Sigma-Aldrich) in a final volume of 1 mL of RPMI at 37°C for 30 min under agitation. Single cells were isolated, counted, extracellular and intracellular staining were performed. Anti-CD16/CD32 antibodies was used (2.4G2; BD Biosciences) to avoid nonspecific binding. All staining reactions were performed at 4°C for 30 min protected from light. Different subsets of cells were detected by flow cytometry in cell suspensions of lung using a combination of the following fluorochrome-conjugated antibodies against mouse CD45-BV785 (1:200; 30-F11), CD11b-BV605 (1:200; M1/70), CD11c-APC-Cy7 (1:200; N418), F4/80-BV711 (1:200; BM8), TCRβ-BV510 (1:200; H57-597), CD4-BV650 (1:200; RM4-5), CD8α-PerCp-Cy5.5 (1:200; 53-6.7), ICOS (CD278)-Pe-Cy7 (1:200; C398.4A), ST2-BV421 (1:200; DIH9), CD206-APC (1:200; C068C2), MHC-II-BV785 (1:200; M5/114) and Siglec-F-PerCp-Cy5.5 (1:100; S17007L). For IL-13 intracellular staining, cell were then permeabilized using 40μL of cytofix/cytoperm 1X (BDbiosciences®) during 20min at 4°C protected from light. Next, cell were incubated with antibodies against mouse IL-13-APC (1/20; JES10-5A2) during 20min at 4°C protected from light, washed with 200μL of PermWash (BDbiosciences®) and then fixed with 200μL of FACSLysing 1X (BDbiosciences®). For IFNγ *ex vivo* secretion, the kit Mouse IFN-γ Secretion Assay-Detection was used (MACS Miltenyi Biotec®). Briefly, cells were incubated during 30 min with IFN-γ catch reagent diluted in PBS containing 2% FCS plus 2mM EDTA at 37°C. After washing, cells were incubated with IFNγ-PE detection reagent during 30min at 4°C, washed and fixed with FACSLysing 1X as above. FITC Annexin V-PE Propidium Iodide Apoptosis Detection Kit I (BD Bioscience) was used to discriminate live cells to dying/dead cells. Optimal PMT voltages and antibody titrations were performed to properly separate negative and positive staining populations. Flow cytometry analyses were performed on LSR Fortessa X-20 (Becton Dickinson) and FACS CantoII

(Becton Dickinson) flow cytometers. Gating strategy was set up according to FMO control for all antibodies. One million events were recorded. Only singlet cells are presented as discriminated using FSC-A/FSC-H gating strategy. Final analysis and graphical output were performed using FlowJo software (Tree Star, Ashland, OR).

QUANTIFICATION AND STATISTICAL ANALYSIS

Statistical Analysis

Coefficients of correlation (r) were presented as measures of linear association for regression relationships (Spearman's correlation). Statistical analyses were performed using Student's t test, Mann-Whitney U analysis and nonparametric one-way ANOVA with Tukey's post hoc test to determine significant differences between groups. Statistical parameters including the exact value of n, dispersion and precision measures (as mean ± SD or SEM as indicated) and statistical significance are reported in the Figures and Figure legends. In figures asterisks denote statistical significance *$p < 0.05$, **$p < 0.01$, ***$p < 0.001$, ***$p < 0.0001$, ''ns'' = not significant. Statistical tests used are indicated in the figure legends. Statistical analyses for all experiments were performed GraphPad Prism version 6.0 (GraphPad Software, La Jolla, CA). No data were excluded.

DATA AND SOFTWARE AVAILABILITY

All data available from the corresponding authors on request.